



**HAL**  
open science

## Metabolic regulation of ILC2 differentiation into ILC1-like cells during *Mycobacterium tuberculosis* infection

Dan Corral, Alison Charton, Maria Z Krauss, Eve Blanquart, Florence Levillain, Emma Lefrançais, Tamara Sneperger, Jean-Philippe Girard, Gérard Eberl, Yannick Poquet, et al.

### ► To cite this version:

Dan Corral, Alison Charton, Maria Z Krauss, Eve Blanquart, Florence Levillain, et al.. Metabolic regulation of ILC2 differentiation into ILC1-like cells during *Mycobacterium tuberculosis* infection. 2021. hal-03451521

**HAL Id: hal-03451521**

**<https://hal.science/hal-03451521v1>**

Preprint submitted on 26 Nov 2021

**HAL** is a multi-disciplinary open access archive for the deposit and dissemination of scientific research documents, whether they are published or not. The documents may come from teaching and research institutions in France or abroad, or from public or private research centers.

L'archive ouverte pluridisciplinaire **HAL**, est destinée au dépôt et à la diffusion de documents scientifiques de niveau recherche, publiés ou non, émanant des établissements d'enseignement et de recherche français ou étrangers, des laboratoires publics ou privés.

Copyright

# 1 **Metabolic regulation of ILC2 differentiation into** 2 **ILC1-like cells during *Mycobacterium tuberculosis*** 3 **infection**

4 Dan Corral<sup>1,2#</sup>, Alison Charton<sup>1</sup>, Maria Z Krauss<sup>3</sup>, Eve Blanquart<sup>4</sup>, Florence Levillain<sup>1</sup>,  
5 Emma Lefrançais<sup>1</sup>, Tamara Sneider<sup>1</sup>, Jean-Philippe Girard<sup>1</sup>, Gérard Eberl<sup>5</sup>, Yannick  
6 Poquet<sup>1</sup>, Jean-Charles Guéry<sup>4</sup>, Rafael J Arguello<sup>6</sup>, Matthew R Hepworth<sup>3</sup>, Olivier  
7 Neyrolles<sup>1,7</sup> and Denis Hudrisier<sup>1,7#</sup>

8 <sup>1</sup>Institut de Pharmacologie et Biologie Structurale, IPBS, Université de Toulouse, CNRS, UPS,  
9 Toulouse, France

10 <sup>2</sup>Present address: Metaorganism Immunity Section, Laboratory of Host Immunity and Microbiome,  
11 National Institute of Allergy and Infectious Diseases, National Institutes of Health, Bethesda, MD, USA

12 <sup>3</sup>Lydia Becker Institute of Immunology and Inflammation, Division of Infection, Immunity and  
13 Respiratory Medicine, School of Biological Sciences, Faculty of Biology, Medicine and Health,  
14 Manchester Academic Health Science Centre, University of Manchester, Manchester, M13 9PL, UK

15 <sup>4</sup>Institut Toulousain des Maladies Infectieuses et Inflammatoires (INFINITY), Université de Toulouse,  
16 CNRS, UPS, Toulouse, France

17 <sup>5</sup>Institut Pasteur, Microenvironnement & Immunity Unit, 75724 Paris, France ; INSERM U1224, 75724  
18 Paris, France

19 <sup>6</sup>Aix Marseille Univ, CNRS, INSERM, CIML, Centre d'Immunologie de Marseille-Luminy, Marseille,  
20 France

21 <sup>7</sup>These authors contributed equally: Olivier Neyrolles, Denis Hudrisier

22 #Co-corresponding authors: Dan Corral ([dan.corral@nih.gov](mailto:dan.corral@nih.gov)); Denis Hudrisier  
23 ([denis.hudrisier@ipbs.fr](mailto:denis.hudrisier@ipbs.fr))

24 **Abstract**

25 Tissue-resident innate lymphoid cells (ILCs) regulate tissue homeostasis, protect  
26 against pathogens at mucosal surfaces and are key players at the interface of innate  
27 and adaptive immunity. How ILCs adapt their phenotype and function to environmental  
28 cues within tissues remains to be fully understood. Here, we show that *Mycobacterium*  
29 *tuberculosis* infection alters the phenotype and function of immature lung ILC2 toward  
30 a protective interferon- $\gamma$ -producing ILC1-like population. This differentiation is  
31 controlled by type 1 cytokines and is associated with a glycolytic program involving the  
32 transcription factor HIF1 $\alpha$ . Collectively, our data reveal how tissue-resident ILCs adapt  
33 to type 1 inflammation toward a pathogen tailored immune response.

## 34 Introduction

35 Innate lymphoid cells (ILCs) are a population of tissue-resident cells of lymphoid origin  
36 that play a key part in both tissue homeostasis and immunity. ILCs are subdivided into  
37 three distinct populations based on their expression of cytokines and specific  
38 transcription factors. ILC1 depend on T-bet and produce interferon (IFN)- $\gamma$ , ILC2  
39 depend on GATA3 and produce interleukin (IL)-5 and IL-13, and ILC3 depend on  
40 ROR $\gamma$ t and produce IL-17A and IL-22 (Meininger et al., 2020; Vivier et al., 2018). Based  
41 on these properties, group 1, 2 and 3 ILCs are commonly presented as the innate  
42 counterparts of T helper type 1 (Th1), Th2 and Th17 cells, contributing to type 1, 2 and  
43 3 immune responses, respectively.

44 The regulome of ILCs evolves progressively during the development of each  
45 population to reach a state in which key loci specific to each lineage are acquired (Shih  
46 et al., 2016; Vivier et al., 2016). Yet, several elements controlling cytokine expression  
47 or loci encoding lineage-determining transcription factors remain broadly accessible in  
48 all ILC subsets (Shih et al., 2016). This feature contributes to the remarkable ability of  
49 ILCs to dynamically adapt to physiological or pathological alterations in their tissue of  
50 residence, and to adopt new phenotypic and functional profiles. Besides the local  
51 plasticity among mature ILC subsets (Bal et al., 2020), circulatory and tissue resident  
52 ILC precursors in human and mouse contribute to the local differentiation into mature  
53 ILCs, an “*ILCpoiesis*” *in situ* (Lim and Di Santo, 2019), sustaining the ILC response  
54 depending on tissue and inflammation (Ghaedi et al., 2020; Lim et al., 2017; Zeis et  
55 al., 2020). While the various populations of tissue-resident ILCs can promptly sense  
56 and adapt to environmental changes (Meininger et al., 2020; Ricardo-Gonzalez et al.,  
57 2018) the mechanism allowing such responses remains to be fully elucidated.

58 In both mice and human subjects, *Mycobacterium tuberculosis* (*Mtb*) infection  
59 induces prolonged proinflammatory responses that are associated with oxidative  
60 stress, which favors tissue destruction and triggers a tissue remodeling program. *Mtb*  
61 infection is also associated with metabolic changes in the lungs, involving the utilization  
62 of aerobic glycolysis primarily instead of oxidative phosphorylation (OXPHOS) in  
63 mitochondria (Warburg effect) (Fernández-García et al., 2020; Shi et al., 2015). At the  
64 cytokine level, the lungs at steady-state mostly host resting ILC2, which, together with  
65 alveolar macrophages, imprint a type 2-oriented environment to the tissue (Saluzzo et  
66 al., 2017; Svedberg et al., 2019). *Mtb* infection of the lung triggers dramatic changes

67 leading to the development of type 1 immunity that is mediated by IFN- $\gamma$  and is  
68 associated with protection (O'Garra et al., 2013).

69 Here, using the murine model of *Mtb* infection, we explored how lung ILCs respond  
70 to chronic pulmonary infection and, in particular, how ILC subsets adapt and respond  
71 to type 1 inflammation within tissue. Our work uncovers the local differentiation of lung  
72 ILC2 precursors into a protective ILC1-like population through metabolic regulation  
73 during *Mtb* infection.

74

## 75 **Results and Discussion**

### 76 **Local differentiation of ILC2 precursor into ILC1-like cells during *Mtb* infection**

77 In order to investigate how a chronic type 1 infection impacts lung ILC subsets,  
78 C57BL/6 mice were infected with the *Mtb* reference strain H37Rv. At steady-state,  
79 *bona fide* lung ILCs were defined as a population that does not express lineage  
80 markers (CD3, CD4, CD8, TCR $\beta$ , TCR $\alpha\delta$ , CD49b, CD11b, CD11c, B220, CD19,  
81 F4/80, GR-1, TER119, Fc $\epsilon$ R1a) but highly express CD90.2 and CD45.2 (**Figure 1A**).  
82 ILC2 (GATA3<sup>high</sup>), which represent the major ILC population in the murine lung, were  
83 identified after exclusion of ILC1 (NK1.1<sup>+</sup>) and ILC3 (ROR $\gamma$ t<sup>+</sup>) cells (**Figure 1A**). At  
84 steady state, and in agreement with previously published work (Stehle et al., 2018;  
85 Vivier et al., 2018), the lung is dominantly enriched in ILC2 (**Figure 1A and 1B**).  
86 Notably, a small frequency of ILC2 expressed IL-18R $\alpha$  (**Figure 1B**), a phenotype  
87 previously utilized to identify tissue-resident ILC precursor (ILCP) able to differentiate  
88 into ILC2 in the context of type 2 inflammatory responses (Ghaedi et al., 2020; Zeis et  
89 al., 2020). IL-18R $\alpha$ <sup>+</sup> ILC2 expressed canonical ILC2 markers such as GATA3, ST2,  
90 and Arg1 at lower levels than IL-18R $\alpha$ <sup>-</sup> ILC2 (**Supplementary Figure 1A-B**). At the  
91 functional level, these cells produced lower amount of IL-5 compared to IL-18R $\alpha$ <sup>-</sup> ILC2  
92 and did not produce IFN- $\gamma$  like ILC1 (**Supplementary Figure 1C**). In line with previous  
93 studies (Ghaedi et al., 2020; Zeis et al., 2020), we found that IL-18R $\alpha$ <sup>+</sup> ILC2 express  
94 high levels of TCF-1, like ILC2 precursors from the bone marrow, confirming their  
95 immature profile (**Supplementary Figure 1D**). *Mtb* infection had a profound impact on  
96 ILC composition and phenotype and was associated with gradual increase in ILC1 and  
97 ILC3 (**Supplementary Figure 1E**). Of particular interest, *Mtb* infection promoted the

98 accumulation of a novel ILC population expressing both IL-18R $\alpha$  and T-bet within the  
99 lung (**Figure 1A and 1B**) and concomitant reduction in IL-18R $\alpha$ <sup>-</sup> ILC2 (**Supplementary**  
100 **Figure 1E**). Phenotypical analysis revealed that this subset displayed little to no  
101 classical ILC2 markers, such as GATA3, ST2, Arg1 and IL-5 (**Figure 1C**), or ILC3  
102 markers, such as ROR $\gamma$ t (**Figure 1A**). Like ILC1, this subset expressed T-bet, CD49a,  
103 and CD226 (**Figure 1D**) but did not express NK1.1 (gated on NK1.1 negative ILCs),  
104 NKp46 or Eomes (**Figure 1A; Supplementary Figure 1E**). At the functional level, we  
105 found that this population was able to produce IFN- $\gamma$ , but not IL-5 or IL-17A (**Figure**  
106 **1E**). We therefore named this new subset “ILC1-like cells”, based on the similarities  
107 (**Figure 1D and 1E**) and differences (**Figure 1A; Supplementary Figure 1F**) with NK  
108 cells/ILC1. ILC1-like cells became detectable after 21 days of infection and expanded  
109 in the following weeks (**Figure 1F**). Adaptive immune responses are detectable within  
110 the lung at 21 days post-*Mtb* infection (Urdahl et al., 2011), which coincides with the  
111 detection of ILC1-like cells. As such we assessed the role of adaptive immunity in the  
112 emergence of this ILC subset. ILC1-like cells were detectable in *Mtb* infected *Rag2*<sup>-/-</sup>  
113 mice that lack adaptive immunity, and at a higher level that in infected wild-type mice.  
114 Thus, adaptive immunity is not required for the generation of ILC1-like cells following  
115 infection (**Supplementary Figure 1G**).

116 ILCs have been reported to adapt their profile to environmental cues. Different  
117 mechanisms have been described to sustain the local adaptation of ILCs during  
118 inflammation such as plasticity of mature ILC subsets (Bal et al., 2020), *in situ*  
119 differentiation of ILC precursor (Ghaedi et al., 2020; Zeis et al., 2020) as well as the  
120 migration of ILC from bone marrow (Zeis et al., 2020). Furthermore, ILCs with  
121 characteristics of ILC1-like cells have been shown to arise from various ILC subsets  
122 through mechanisms of plasticity depending on the tissue and the inflammatory context  
123 (Bal et al., 2020; Silver et al., 2016). In the lungs, ILC2 have been described to acquire  
124 expression of T-bet, IL-18R $\alpha$  and IFN- $\gamma$  during influenza virus infection (Silver et al.,  
125 2016). We hypothesized that ILC1-like cells could differentiate from lung ILC2. To  
126 assess if ILC2 display plasticity during *Mtb* infection, we adoptively transferred total  
127 lung ST2<sup>+</sup> ILC2, sorted regardless of their IL-18R $\alpha$  expression, into *Rag2*<sup>-/-</sup>*Ii2rg*<sup>-/-</sup> mice,  
128 which are devoid of T cells, B cells and NK/ILCs, one day prior to *Mtb* infection  
129 (**Supplementary Figure 1H and 1I**). Before transfer, we confirmed that sorted ILC2  
130 expressed GATA3 but not T-bet or ROR $\gamma$ t (**Supplementary Figure 1J**) and noticed

131 that IL-18R $\alpha$  expression was lost during *in vitro* culture (**Supplementary Figure 1J**).  
132 Following transfer, ILC2 strongly upregulated T-bet in infected, but not in non-infected  
133 mice (**Supplementary Figure 1K and 1L**). Furthermore, T-bet<sup>high</sup> cells expressed  
134 higher level of IL-18R $\alpha$  and Ki67 compared to GATA3<sup>high</sup> cells (**Supplementary Figure**  
135 **1M**). Given that ILC2 can give rise to ILC1-like cells, we sought to explore which ILC2  
136 subset preferentially differentiated into ILC1-like cells. Intriguingly, while IL-18R $\alpha$ <sup>+</sup> ILC2  
137 did not acquire ILC1 markers during *Mtb* infection (**Figure 1D**) and accumulate into the  
138 lungs (**Figure 1G**), they gained the potential to produce IFN- $\gamma$  and did not produce IL-  
139 5 (**Figure 1E**). Moreover, IL-18R $\alpha$ <sup>+</sup> ILC2, unlike ILC1 and ILC1-like cells, did not  
140 respond to *ex vivo* stimulation with IL-12 and IL-18 (**Figure 1H**). Thus, we hypothesized  
141 that this population could have the potential to differentiate into ILC1-like cells and  
142 could thus represent an early stage of ILC1-like. We assessed if IL-18R $\alpha$ <sup>+</sup> ILC2 have  
143 the potential to differentiate into ILC1-like during *Mtb* infection. To this end, we sorted  
144 ILC2 subsets from IL-33 treated mice based on their IL-18R $\alpha$  expression and  
145 adoptively transferred them into *Rag2*<sup>-/-</sup>*Il2rg*<sup>-/-</sup> mice one day before infection with *Mtb*  
146 (**Figure 1I**). Interestingly, we found that the transfer of IL-18R $\alpha$ <sup>+</sup> ILC2 resulted in higher  
147 proportions of ILC in the lungs when compared to the conditions where the same  
148 number of IL-18R $\alpha$ <sup>-</sup> ILC2 were transferred (**Figure 1J**); in addition, T-bet expression  
149 among IL-18R $\alpha$ <sup>+</sup> ILC2 was significantly increased in the former case (**Figure 1K**).  
150 Thus, IL-18R $\alpha$ <sup>+</sup> ILC2, rather than IL-18R $\alpha$ <sup>-</sup> ILC2, have the potential to differentiate into  
151 ILC1-like cells during *Mtb* infection.

152 Altogether, our data show that *Mtb* infection differentially impacts the composition  
153 of ILC subsets within the lung, and especially induces the local differentiation of lung  
154 ILC2 precursor into a ILC1-like cell population.

## 155 **Type 1 inflammatory environment shapes the fate of IL-18R $\alpha$ <sup>+</sup> ILC2**

156 Next, we aimed to assess how the inflammatory milieu influences the fate of IL-18R $\alpha$ <sup>+</sup>  
157 ILC2. *Mtb* infection triggers the development of a type 1 immunity (O'Garra et al.,  
158 2013). Both IL-12 and IL-18 contribute in the establishment of this type 1 inflammatory  
159 environment (Kinjo et al., 2002; O'Garra et al., 2013) in particular by inducing the  
160 expression of IFN- $\gamma$  on ILC1, NK cells and Th1 (Chiossone et al., 2018; Weizman et  
161 al., 2017). Therefore, we administered to mice IL-12 and IL-18 intranasally for 1 week

162 and found that this treatment was sufficient to induce the accumulation of ILC1-like  
163 cells in the lungs (**Figure 2A-B**). Furthermore IL-18R $\alpha^+$  ILC2 also expanded in these  
164 settings (**Figure 2B**) and lost the expression of TCF-1 (**Figure 2C**), supporting the idea  
165 that these cells may underwent a local differentiation process. Similarly, to *Mtb*  
166 infection, IL-18R $\alpha^+$  ILC2, and IL-18R $\alpha^-$  ILC2, lost their ability to produce IL-5 following  
167 cytokine injection and acquired the ability to produce IFN- $\gamma$  (**Figure 2D**), but not after  
168 *ex vivo* stimulation with IL-12 and IL-18 (**Figure 2E**). Moreover, we crossed IL-5<sup>Cre-</sup>  
169 <sup>tdTomato</sup> (Red5) mice with ROSA26-YFP mice to enable fate-mapping mature ILC2  
170 (Nussbaum et al., 2013) and that the majority of ILC1-like cell do not derive from IL-  
171 18R $\alpha^-$  ILC2, the only ILC population expressing IL-5 at steady-state and during type 1  
172 inflammation (**Supplementary Figure 2A-B**), reinforcing our previous observation  
173 (**Figure 1J**). Overall, based on the expression of several markers (GATA3, Arg1, T-  
174 bet, IL-18R $\alpha$ , CD49a, CD226 and Ki67), we found close similarities in both IL-18R $\alpha^+$   
175 ILC2 and ILC1-like cells generated upon either IL-12/IL-18 treatment or during *Mtb*  
176 infection (**Supplementary Figure 2B**). Thus, the generation of ILC1-like cells  
177 observed during *Mtb* infection can be closely recapitulated with the simple  
178 administration of IL-12 and IL-18.

179 To further demonstrate the ILC2 origin of ILC1-like cells during type 1 inflammation,  
180 we studied the effect of IL-33, a well-known inducer of both mature and immature ILC2  
181 (Moro et al., 2010; Neill et al., 2010; Price et al., 2010), on ILC1-like differentiation. IL-  
182 33 alone did not induce the differentiation of ILC1-like cells, although it did induce a  
183 high expansion of mature and immature ILC2 (**Figure 2F-I**). In association with IL-12  
184 and IL-18, IL-33 was able to enhance ILC1-like differentiation (**Figure 2I** and  
185 **Supplementary Figure 2C**). Intriguingly, while IL-18R $\alpha^+$  ILC2 expressed ILC2  
186 markers (ST2, Arg1 and IL-5) in IL-33-treated mice (**Figure 2J-K**), and ILC1-like  
187 markers (CD49a, IFN- $\gamma$ ) in IL-12/IL-18-treated animals (**Figure 2J-K**), the combination  
188 of IL-12/IL-18 with IL-33 led to a mixed ILC1/ILC2 phenotype with the capacity to  
189 produce both IL-5 and IFN- $\gamma$ . Because ST2 is expressed by various cell types, including  
190 ILC2, we also tested Neuromedin U (NMU), whose receptor is solely present in bone  
191 marrow ILC2P and in lung ILC2 (Cardoso et al., 2017; Klose et al., 2014; Wallrapp et  
192 al., 2017). Similar to IL-33, NMU potentiated the differentiation of ILC1-like cells  
193 induced by IL-12 and IL-18 (**Figure 2L**). Altogether, these results demonstrate that  
194 lung IL-18R $\alpha^+$  ILC2 exhibit a highly adaptable phenotype, dependent on the



195 inflammatory environment. While they strengthen the ILC2 response in a type 2  
196 environment (*i.e.*, after administration of IL-33), these cells rather differentiate into IFN-  
197  $\gamma$ -producing ILC1-like cells in a type 1 environment (*i.e.*, after administration of IL-12  
198 and IL-18). This result supports the recent notion that local ILC precursors may  
199 undergo “*ILCpoiesis*” (Ghaedi et al., 2020; Zeis et al., 2020), as demonstrated in  
200 human (Lim et al., 2017; Lim and Di Santo, 2019). Although we cannot exclude local  
201 plasticity of other ILC subsets, or ILCP recruitment from the bone marrow, our results  
202 strongly suggest the local differentiation of lung ILC2P into ILC1-like cells during type  
203 1 inflammation.

### 204 **ILC1-like cell differentiation is associated with a metabolic reprogramming** 205 **toward glycolysis.**

206 Recent RNA-sequencing analyses of intestinal ILCs revealed that each subset  
207 display unique metabolic profiles (Gury-BenAri et al., 2016). While the need in amino  
208 acid metabolism for lung ILC2 functions relies on Arg1 (Monticelli et al., 2016), the  
209 glycolytic pathway necessary for ILC3 functions depends on mTOR and HIF1 $\alpha$  (Di  
210 Luccia et al., 2019). However, little is known about metabolic adaptation of ILCs to their  
211 environment during infection (Joseph et al., 2018). Fate decisions of immune cells such  
212 as those underlying differentiation of Treg/Th17 or Treg/Th1 have been tightly  
213 associated with metabolic reprogramming (Clever et al., 2016; Dang et al., 2011; Shi  
214 et al., 2011). Given that IL-18R $\alpha^+$  ILC2 present the ability to differentiate into ILC1-like  
215 cells in a type 1 inflammatory context, we investigated the metabolic pathways  
216 engaged during ILC1-like cells differentiation. To gain insight in ILC metabolism, we  
217 took advantage of the recently described SCENITH method (Argüello et al., 2020),  
218 which allows to determine global metabolic dependencies and capacities at the single  
219 cell level. SCENITH uses protein synthesis levels as a readout and is particularly  
220 appropriate to analyze the metabolism of rare cells, such as ILCs. ILC1-like cells were  
221 compared to control cells known to rely on a glycolytic metabolism (*e.g.*, NK cells) and  
222 to ILC2 in lungs. In agreement with the inhibitory effect of type 1 inflammation on IL-  
223 18R $\alpha^-$  ILC2 (**Figure 1E; Supplementary Figure 1F**), administration of IL-12 and IL-18  
224 downregulated ILC2 global level of translation, as assessed via detection of puromycin  
225 incorporation (**Figure 3A-C**). Conversely, following cytokine injection, the level of  
226 translation was increased in NK cells, IL-18R $\alpha^+$  ILC2 and ILC1-like cells with the latter

227 cells displaying the highest rate (**Figure 3A-C**). Notably, a similar pattern was observed  
228 during *Mtb* infection (**Supplementary Figure 3A**). The analysis of protein synthesis in  
229 the presence of inhibitors targeting different metabolic pathways, namely 2-DG for  
230 glycolysis and oligomycin for OXPHOS, allowed us to assess the mitochondrial  
231 dependence and glycolytic capacity of the cells (**Figure 3D**). We found that, in all ILC  
232 subsets tested, type 1 inflammation led to a global decrease in their mitochondrial  
233 dependence, together with an increase in their glycolytic capacity, that is a canonical  
234 feature of the Warburg effect (Heiden et al., 2009) (**Figure 3E and F**). Thus, while a  
235 metabolic reprogramming towards glycolysis is significantly induced in IL-18R $\alpha$ <sup>-</sup> ILC2,  
236 IL-18R $\alpha$ <sup>+</sup> ILC2 and characterized ILC1-like cells upon type 1 inflammation, this  
237 program was also associated with a global inhibition of IL-18R $\alpha$ <sup>-</sup> ILC2 compared to the  
238 other ILC subsets tested. Arg1 has been previously identified as a critical component  
239 of the metabolic programming of lung ILC2, with its inhibition or genetic inactivation  
240 resulting in reduced aerobic glycolysis (Monticelli et al., 2016). In agreement with  
241 previous studies (Bando et al., 2013; Monticelli et al., 2016; Schneider et al., 2019),  
242 we found that Arg1 was highly expressed in both IL-18R $\alpha$ <sup>-</sup> and IL-18R $\alpha$ <sup>+</sup> ILC2 (**Figure**  
243 **3G**). However, after treatment with IL-12 and IL-18, the expression of Arg1 decreased  
244 in IL-18R $\alpha$ <sup>+</sup> ILC2 to similar level as ILC1-like cells, supporting the idea that Arg1 is not  
245 implicated in the metabolic regulation of ILC1-like cell differentiation. Previous work  
246 proposed that the Warburg effect, a metabolic pathway that is engaged during *Mtb*  
247 infection (Fernández-García et al., 2020; Shi et al., 2015), relies on the transcription  
248 factor hypoxia-inducible factor-1  $\alpha$  (HIF1 $\alpha$ ) (Palazon et al., 2014). Of interest, in a  
249 model of von Hippel-Lindau (VHL) deficiency, where HIF1 $\alpha$  is overexpressed, it was  
250 previously shown that ILC2 development was repressed through glycolysis induction  
251 (Li et al., 2018). These observations prompted us to analyze HIF1 $\alpha$  expression in our  
252 model. Type 1 inflammation driven by IL-12/IL-18 treatment led to the induction of  
253 HIF1 $\alpha$  in both IL-18R $\alpha$ <sup>-</sup> and IL-18R $\alpha$ <sup>+</sup> ILC2, and in ILC1-like cells (**Figure 3H**). Given  
254 that IL-18R $\alpha$ <sup>-</sup> and IL-18R $\alpha$ <sup>+</sup> ILC2 share the same metabolic dependence but differ in  
255 their activation state during type 1 inflammation, we analyzed the impact of HIF1 $\alpha$   
256 expression on ILC2. We performed an *in vitro* assay using sorted ILC2 cultured in the  
257 presence of DMOG, which stabilizes the HIF1 $\alpha$  protein (Palazon et al., 2014) (**Figure**  
258 **3I**). DMOG-treatment had a significant inhibitory impact on expression of ILC2 markers  
259 including GATA3, ST2 and IL-5 (**Figure 3J-L**). Accordingly, analysis of the global

260 metabolic profile of ILC2 revealed that DMOG-treated ILC2 harbored a glycolytic profile  
261 (**Figure 3M**), while untreated ILC2 preferentially used mitochondrial respiration  
262 (**Figure 3N**). Most notably, DMOG treatment alone was sufficient to upregulate genes  
263 typically associated with an ILC1 phenotype, such as *Tbx21*, *Ifng* and *Ii18r1* (**Figure**  
264 **3O**). Altogether, these results suggest that HIF1 $\alpha$  in lung ILC2 promote a metabolic  
265 reprogramming toward glycolysis, while favoring the acquisition of an ILC1-like profile.

266 Next, we sought to determine the role of glycolysis in the differentiation of ILC1-  
267 like cells during *Mtb* infection. First, we observed that HIF1 $\alpha$  is expressed in all ILC  
268 subsets, with the highest levels in ILC3 and ILC1-like cells (**Supplementary Figure**  
269 **3B**). Inhibition of glycolysis during *ex vivo* stimulation of total lung ILCs decreased the  
270 proportion of IFN- $\gamma$ <sup>+</sup> ILCs (**Supplementary Figure 3C**), showing that IFN- $\gamma$  production  
271 is glycolysis-dependent. To assess the impact of glycolysis induction *in vivo*, we first  
272 treated mice with 2-deoxyglucose (2-DG), a glycolysis inhibitor, during *Mtb* infection.  
273 2-DG administration markedly decreased the number of ILC1-like cells as well as their  
274 ability to produce IFN- $\gamma$  (**Supplementary Figure 3D, E**). Next, since glucose is  
275 consumed in the lungs of *Mtb*-infected mice (Fernández-García et al., 2020), we  
276 investigated if the modulation of glucose availability in the lung environment could  
277 modulate the differentiation of ILC1-like cells. Glucose supplementation in the animals'  
278 drinking water enhanced the differentiation of ILC1-like cells (**Supplementary Figure**  
279 **3F**) and increased the percentage of IFN- $\gamma$ <sup>+</sup> ILC1-like cells (**Supplementary Figure**  
280 **3G**). Thus, these results strongly suggest that glycolysis is required to support ILC1-  
281 like cells differentiation and function during *Mtb* infection.

282

### 283 **ILC1-like cells confer protection against *Mtb***

284 Next, we investigated whether BCG, the only available vaccine for TB, might impact  
285 the population of lung-resident ILCs when delivered intranasally, a route providing a  
286 better protection than the conventional subcutaneous route (Perdomo et al., 2016),  
287 prior to *Mtb* infection (**Figure 4A**). As expected, mucosal BCG vaccination induced  
288 protection upon *Mtb* challenge (**Figure 4B**). In vaccinated mice, protection correlated  
289 with an increase in T-bet expression in ILCs (**Figure 4C**). More importantly, although  
290 BCG vaccination had no impact on other ILC subsets (**Figure 4D**), higher numbers of  
291 ILC1-like cells were detected at 14 days post-infection, a time when IFN- $\gamma$  -producing

292 ILC1-like cells were virtually absent from non-vaccinated mice (**Figure 4D, E**) but well-  
293 induced in vaccinated animals (**Figure 4D, E**). Overall, BCG vaccination promotes  
294 ILC1-like cells in early stages of infection, which could contribute to protection against  
295 *Mtb*.

296 Finally, to assess the contribution of ILC1-like cells to protection against *Mtb*, we  
297 took advantage of the cytokine-induced ILC1-like cell model (**Figure 4F**) to generate  
298 enough ILC1-like cells for adoptive transfer. ILC1-like cells were sorted from the lungs  
299 of mice treated with IL-12, IL-18 and IL-33; these cells expressed T-bet, but not GATA3  
300 or ROR $\gamma$ t (**Figure 4G**). Remarkably, the transfer of as few as 10,000 ILC1-like cells  
301 resulted in a statistically significant reduction in bacterial load after *Mtb* challenge,  
302 demonstrating the protective capacity of ILC1-like cells against the tuberculosis  
303 bacillus (**Figure 4H**). Recently, ILC3 were reported to mediate protection against *Mtb*  
304 through induction of lung ectopic lymphoid follicles (Ardain et al., 2019). Although our  
305 results confirm the expansion and activation of ILC3 during *Mtb* infection (**Figure 1E** ;  
306 **Supplementary Figure 1F**), we report the expansion of an ILC1-like cell population,  
307 which can contribute to protection against *Mtb* infection. Differences between the two  
308 studies may be due to the *Mtb* strains used, namely HN878 (Ardain et al., 2019) vs.  
309 H37Rv in our study, the different proportions of the various ILC subsets found in the  
310 lungs, or both. In particular, infection with the hypervirulent strain HN878 is known to  
311 induce a different inflammatory pattern (e.g. with strong production of IL-1 $\beta$  and type 1  
312 IFN) and protective immune mechanisms (e.g. IL-17 and IL-22 production) compared  
313 to H37Rv (Gopal et al., 2014; Manca et al., 2001). Thus, depending on the strain and  
314 the associated inflammation, ILC subsets might be highly impacted in their regulation  
315 and function during infection.

316 Thus, we propose a model in which the local differentiation of lung ILC2 precursor into  
317 ILC1-like cells is regulated by both inflammatory and metabolic environment induced  
318 by *Mtb* infection (**Supplementary Figure 4**). Our observation that BCG vaccination  
319 favors the early generation of ILC1-like cells and that ILC1-like cell are endowed with  
320 a protective potential during *Mtb* infection lead to future studies aiming at elucidating  
321 the role played by ILC1-like cells in protection. On a broader perspective, targeting  
322 ILC1-like cells using dedicated strategies may help develop novel approaches to  
323 combat tuberculosis and other inflammatory diseases.

324 **References**

- 325 Ardain, A., Domingo-Gonzalez, R., Das, S., Kazer, S.W., Howard, N.C., Singh, A.,  
326 Ahmed, M., Nhamoyebonde, S., Rangel-Moreno, J., Ogongo, P., Lu, L., Ramsuran,  
327 D., de la Luz Garcia-Hernandez, M., K. Ulland, T., Darby, M., Park, E., Karim, F.,  
328 Melocchi, L., Madansein, R., Dullabh, K.J., Dunlap, M., Marin-Agudelo, N., Ebihara,  
329 T., Ndung'u, T., Kaushal, D., Pym, A.S., Kolls, J.K., Steyn, A., Zúñiga, J., Horsnell, W.,  
330 Yokoyama, W.M., Shalek, A.K., Kløverpris, H.N., Colonna, M., Leslie, A., Khader, S.A.,  
331 2019. Group 3 innate lymphoid cells mediate early protective immunity against  
332 tuberculosis. *Nature* 570, 528–532. <https://doi.org/10.1038/s41586-019-1276-2>  
333
- 334 Argüello, R.J., Combes, A.J., Char, R., Gigan, J.-P., Baaziz, A.I., Bousiquot, E.,  
335 Camosseto, V., Samad, B., Tsui, J., Yan, P., Boissonneau, S., Figarella-Branger, D.,  
336 Gatti, E., Tabouret, E., Krummel, M.F., Pierre, P., 2020. SCENITH: A Flow Cytometry-  
337 Based Method to Functionally Profile Energy Metabolism with Single-Cell Resolution.  
338 *Cell Metab.* 32, 1063-1075.e7. <https://doi.org/10.1016/j.cmet.2020.11.007>  
339
- 340 Bal, S.M., Golebski, K., Spits, H., 2020. Plasticity of innate lymphoid cell subsets. *Nat.*  
341 *Rev. Immunol.* 1–14. <https://doi.org/10.1038/s41577-020-0282-9>  
342
- 343 Bando, J.K., Nussbaum, J.C., Liang, H.-E., Locksley, R.M., 2013. Type 2 innate  
344 lymphoid cells constitutively express arginase-I in the naïve and inflamed lung. *J.*  
345 *Leukoc. Biol.* 94, 877–884. <https://doi.org/10.1189/jlb.0213084>  
346
- 347 Cardoso, V., Chesné, J., Ribeiro, H., García-Cassani, B., Carvalho, T., Bouchery, T.,  
348 Shah, K., Barbosa-Morais, N.L., Harris, N., Veiga-Fernandes, H., 2017. Neuronal  
349 regulation of type 2 innate lymphoid cells via neuromedin U. *Nature* 549, 277–281.  
350 <https://doi.org/10.1038/nature23469>  
351
- 352 Chiossone, L., Dumas, P.-Y., Vienne, M., Vivier, E., 2018. Natural killer cells and other  
353 innate lymphoid cells in cancer. *Nat. Rev. Immunol.* 18, 671–688.  
354 <https://doi.org/10.1038/s41577-018-0061-z>  
355
- 356 Di Luccia, B., Gilfillan, S., Cella, M., Colonna, M., Huang, S.C.-C., 2019. ILC3s

357 integrate glycolysis and mitochondrial production of reactive oxygen species to fulfill  
358 activation demands. *J. Exp. Med.* 216, 2231–2241.  
359 <https://doi.org/10.1084/jem.20180549>

360

361 Fernández-García, M., Rey-Stolle, F., Boccard, J., Reddy, V.P., García, A., Cumming,  
362 B.M., Steyn, A.J.C., Rudaz, S., Barbas, C., 2020. Comprehensive Examination of the  
363 Mouse Lung Metabolome Following Mycobacterium tuberculosis Infection Using a  
364 Multiplatform Mass Spectrometry Approach. *J. Proteome Res.* 19, 2053–2070.  
365 <https://doi.org/10.1021/acs.jproteome.9b00868>

366

367 Ghaedi, M., Shen, Z.Y., Orangi, M., Martinez-Gonzalez, I., Wei, L., Lu, X., Das, A.,  
368 Heravi-Moussavi, A., Marra, M.A., Bhandoola, A., Takei, F., 2020. Single-cell analysis  
369 of ROR $\alpha$  tracer mouse lung reveals ILC progenitors and effector ILC2 subsets. *J. Exp.*  
370 *Med.* 217. <https://doi.org/10.1084/jem.20182293>

371

372 Gopal, R., Monin, L., Slight, S., Uche, U., Blanchard, E., Fallert Junecko, B.A., Ramos-  
373 Payan, R., Stallings, C.L., Reinhart, T.A., Kolls, J.K., Kaushal, D., Nagarajan, U.,  
374 Rangel-Moreno, J., Khader, S.A., 2014. Unexpected role for IL-17 in protective  
375 immunity against hypervirulent Mycobacterium tuberculosis HN878 infection. *PLoS*  
376 *Pathog.* 10, e1004099. <https://doi.org/10.1371/journal.ppat.1004099>

377

378 Gury-BenAri, M., Thaïss, C.A., Serafini, N., Winter, D.R., Giladi, A., Lara-Astiaso, D.,  
379 Levy, M., Salame, T.M., Weiner, A., David, E., Shapiro, H., Dori-Bachash, M., Pevsner-  
380 Fischer, M., Lorenzo-Vivas, E., Keren-Shaul, H., Paul, F., Harmelin, A., Eberl, G.,  
381 Itzkovitz, S., Tanay, A., Di Santo, J.P., Elinav, E., Amit, I., 2016. The Spectrum and  
382 Regulatory Landscape of Intestinal Innate Lymphoid Cells Are Shaped by the  
383 Microbiome. *Cell* 166, 1231-1246.e13. <https://doi.org/10.1016/j.cell.2016.07.043>

384

385 Heiden, M.G.V., Cantley, L.C., Thompson, C.B., 2009. Understanding the Warburg  
386 Effect: The Metabolic Requirements of Cell Proliferation. *Science* 324, 1029–1033.  
387 <https://doi.org/10.1126/science.1160809>

388

389 Joseph, A.M., Monticelli, L.A., Sonnenberg, G.F., 2018. Metabolic regulation of innate  
390 and adaptive lymphocyte effector responses. *Immunol. Rev.* 286, 137–147.

391 <https://doi.org/10.1111/imr.12703>

392

393 Kinjo, Y., Kawakami, K., Uezu, K., Yara, S., Miyagi, K., Koguchi, Y., Hoshino, T.,  
394 Okamoto, M., Kawase, Y., Yokota, K., Yoshino, K., Takeda, K., Akira, S., Saito, A.,  
395 2002. Contribution of IL-18 to Th1 response and host defense against infection by  
396 *Mycobacterium tuberculosis*: a comparative study with IL-12p40. *J. Immunol. Baltim.*  
397 *Md* 169, 323–329. <https://doi.org/10.4049/jimmunol.169.1.323>

398

399 Klose, C.S.N., Flach, M., Möhle, L., Rogell, L., Hoyler, T., Ebert, K., Fabiunke, C.,  
400 Pfeifer, D., Sexl, V., Fonseca-Pereira, D., Domingues, R.G., Veiga-Fernandes, H.,  
401 Arnold, S.J., Busslinger, M., Dunay, I.R., Tanriver, Y., Diefenbach, A., 2014.  
402 Differentiation of Type 1 ILCs from a Common Progenitor to All Helper-like Innate  
403 Lymphoid Cell Lineages. *Cell* 157, 340–356. <https://doi.org/10.1016/j.cell.2014.03.030>

404

405 Li, Q., Li, D., Zhang, X., Wan, Q., Zhang, W., Zheng, M., Zou, L., Elly, C., Lee, J.H.,  
406 Liu, Y.-C., 2018. E3 Ligase VHL Promotes Group 2 Innate Lymphoid Cell Maturation  
407 and Function via Glycolysis Inhibition and Induction of Interleukin-33 Receptor.  
408 *Immunity* 48, 258-270.e5. <https://doi.org/10.1016/j.immuni.2017.12.013>

409

410 Lim, A.I., Di Santo, J.P., 2019. ILC-poiesis: Ensuring tissue ILC differentiation at the  
411 right place and time. *Eur. J. Immunol.* 49, 11–18. <https://doi.org/10.1002/eji.201747294>

412

413 Lim, A.I., Li, Y., Lopez-Lastra, S., Stadhouders, R., Paul, F., Casrouge, A., Serafini,  
414 N., Puel, A., Bustamante, J., Surace, L., Masse-Ranson, G., David, E., Strick-  
415 Marchand, H., Bourhis, L.L., Cocchi, R., Topazio, D., Graziano, P., Muscarella, L.A.,  
416 Rogge, L., Norel, X., Sallenave, J.-M., Allez, M., Graf, T., Hendriks, R.W., Casanova,  
417 J.-L., Amit, I., Yssel, H., Santo, J.P.D., 2017. Systemic Human ILC Precursors Provide  
418 a Substrate for Tissue ILC Differentiation. *Cell* 168, 1086-1100.e10.  
419 <https://doi.org/10.1016/j.cell.2017.02.021>

420

421 Manca, C., Tsenova, L., Bergtold, A., Freeman, S., Tovey, M., Musser, J.M., Barry,  
422 C.E., Freedman, V.H., Kaplan, G., 2001. Virulence of a *Mycobacterium tuberculosis*  
423 clinical isolate in mice is determined by failure to induce Th1 type immunity and is  
424 associated with induction of IFN- $\alpha/\beta$ . *Proc. Natl. Acad. Sci.* 98, 5752–5757.

425 <https://doi.org/10.1073/pnas.091096998>

426

427 Meininger, I., Carrasco, A., Rao, A., Soini, T., Kokkinou, E., Mjösberg, J., 2020. Tissue-  
428 Specific Features of Innate Lymphoid Cells. *Trends Immunol.* 41, 902–917.

429 <https://doi.org/10.1016/j.it.2020.08.009>

430

431 Monticelli, L.A., Buck, M.D., Flamar, A.-L., Saenz, S.A., Tait Wojno, E.D., Yudanin,  
432 N.A., Osborne, L.C., Hepworth, M.R., Tran, S.V., Rodewald, H.-R., Shah, H., Cross,  
433 J.R., Diamond, J.M., Cantu, E., Christie, J.D., Pearce, E.L., Artis, D., 2016. Arginase  
434 1 is an innate lymphoid-cell-intrinsic metabolic checkpoint controlling type 2  
435 inflammation. *Nat. Immunol.* 17, 656–665. <https://doi.org/10.1038/ni.3421>

436

437 Moro, K., Yamada, T., Tanabe, M., Takeuchi, T., Ikawa, T., Kawamoto, H., Furusawa,  
438 J., Ohtani, M., Fujii, H., Koyasu, S., 2010. Innate production of T H 2 cytokines by  
439 adipose tissue-associated c-Kit + Sca-1 + lymphoid cells. *Nature* 463, 540–544.

440 <https://doi.org/10.1038/nature08636>

441

442 Neill, D.R., Wong, S.H., Bellosi, A., Flynn, R.J., Daly, M., Langford, T.K.A., Bucks, C.,  
443 Kane, C.M., Fallon, P.G., Pannell, R., Jolin, H.E., McKenzie, A.N.J., 2010. Nuocytes  
444 represent a new innate effector leukocyte that mediates type-2 immunity. *Nature* 464,  
445 1367–1370. <https://doi.org/10.1038/nature08900>

446

447 Nussbaum, J.C., Van Dyken, S.J., von Moltke, J., Cheng, L.E., Mohapatra, A.,  
448 Molofsky, A.B., Thornton, E.E., Krummel, M.F., Chawla, A., Liang, H.-E., Locksley,  
449 R.M., 2013. Type 2 innate lymphoid cells control eosinophil homeostasis. *Nature* 502,  
450 245–248. <https://doi.org/10.1038/nature12526>

451

452 O’Garra, A., Redford, P.S., McNab, F.W., Bloom, C.I., Wilkinson, R.J., Berry, M.P.R.,  
453 2013. The Immune Response in Tuberculosis. *Annu. Rev. Immunol.* 31, 475–527.  
454 <https://doi.org/10.1146/annurev-immunol-032712-095939>

455

456 Palazon, A., Goldrath, A.W., Nizet, V., Johnson, R.S., 2014. HIF Transcription Factors,  
457 Inflammation, and Immunity. *Immunity* 41, 518–528.

458 <https://doi.org/10.1016/j.immuni.2014.09.008>



- 459 Perdomo, C., Zedler, U., Köhl, A.A., Lozza, L., Saikali, P., Sander, L.E., Vogelzang,  
460 A., Kaufmann, S.H.E., Kupz, A., 2016. Mucosal BCG Vaccination Induces Protective  
461 Lung-Resident Memory T Cell Populations against Tuberculosis. *mBio* 7.  
462 <https://doi.org/10.1128/mBio.01686-16>  
463
- 464 Price, A.E., Liang, H.-E., Sullivan, B.M., Reinhardt, R.L., Eisle, C.J., Erle, D.J.,  
465 Locksley, R.M., 2010. Systemically dispersed innate IL-13-expressing cells in type 2  
466 immunity. *Proc. Natl. Acad. Sci.* 107, 11489–11494.  
467 <https://doi.org/10.1073/pnas.1003988107>  
468
- 469 Ricardo-Gonzalez, R.R., Van Dyken, S.J., Schneider, C., Lee, J., Nussbaum, J.C.,  
470 Liang, H.-E., Vaka, D., Eckalbar, W.L., Molofsky, A.B., Erle, D.J., Locksley, R.M., 2018.  
471 Tissue signals imprint ILC2 identity with anticipatory function. *Nat. Immunol.* 19, 1093–  
472 1099. <https://doi.org/10.1038/s41590-018-0201-4>  
473
- 474 Saluzzo, S., Gorki, A.-D., Rana, B.M.J., Martins, R., Scanlon, S., Starkl, P., Lakovits,  
475 K., Hladik, A., Korosec, A., Sharif, O., Warszawska, J.M., Jolin, H., Mesteri, I.,  
476 McKenzie, A.N.J., Knapp, S., 2017. First-Breath-Induced Type 2 Pathways Shape the  
477 Lung Immune Environment. *Cell Rep.* 18, 1893–1905.  
478 <https://doi.org/10.1016/j.celrep.2017.01.071>  
479
- 480 Schneider, C., Lee, J., Koga, S., Ricardo-Gonzalez, R.R., Nussbaum, J.C., Smith, L.K.,  
481 Villeda, S.A., Liang, H.-E., Locksley, R.M., 2019. Tissue-Resident Group 2 Innate  
482 Lymphoid Cells Differentiate by Layered Ontogeny and In Situ Perinatal Priming.  
483 *Immunity* 50, 1425-1438.e5. <https://doi.org/10.1016/j.immuni.2019.04.019>  
484
- 485 Shi, L., Salamon, H., Eugenin, E.A., Pine, R., Cooper, A., Gennaro, M.L., 2015.  
486 Infection with *Mycobacterium tuberculosis* induces the Warburg effect in mouse lungs.  
487 *Sci. Rep.* 5, 1–13. <https://doi.org/10.1038/srep18176>  
488
- 489 Shih, H.-Y., Sciumè, G., Mikami, Y., Guo, L., Sun, H.-W., Brooks, S.R., Urban, J.F.,  
490 Davis, F.P., Kanno, Y., O’Shea, J.J., 2016. Developmental Acquisition of Regulomes  
491 Underlies Innate Lymphoid Cell Functionality. *Cell* 165, 1120–1133.  
492 <https://doi.org/10.1016/j.cell.2016.04.029>

- 493 Silver, J.S., Kearley, J., Copenhaver, A.M., Sanden, C., Mori, M., Yu, L., Pritchard,  
494 G.H., Berlin, A.A., Hunter, C.A., Bowler, R., Erjefalt, J.S., Kolbeck, R., Humbles, A.A.,  
495 2016. Inflammatory triggers associated with exacerbations of COPD orchestrate  
496 plasticity of group 2 innate lymphoid cells in the lungs. *Nat. Immunol.* 17, 626–635.  
497 <https://doi.org/10.1038/ni.3443>  
498
- 499 Svedberg, F.R., Brown, S.L., Krauss, M.Z., Campbell, L., Sharpe, C., Clausen, M.,  
500 Howell, G.J., Clark, H., Madsen, J., Evans, C.M., Sutherland, T.E., Ivens, A.C.,  
501 Thornton, D.J., Grecis, R.K., Hussell, T., Cunoosamy, D.M., Cook, P.C., MacDonald,  
502 A.S., 2019. The lung environment controls alveolar macrophage metabolism and  
503 responsiveness in type 2 inflammation. *Nat. Immunol.* 20, 571–580.  
504 <https://doi.org/10.1038/s41590-019-0352-y>  
505
- 506 Troegeler, A., Mercier, I., Cougoule, C., Pietretti, D., Colom, A., Duval, C., Vu Manh,  
507 T.-P., Capilla, F., Poincloux, R., Pingris, K., Nigou, J., Rademann, J., Dalod, M.,  
508 Verreck, F.A.W., Al Saati, T., Lugo-Villarino, G., Lepenies, B., Hudrisier, D., Neyrolles,  
509 O., 2017. C-type lectin receptor DCIR modulates immunity to tuberculosis by  
510 sustaining type I interferon signaling in dendritic cells. *Proc. Natl. Acad. Sci. U. S. A.*  
511 114, E540–E549. <https://doi.org/10.1073/pnas.1613254114>  
512
- 513 Urdahl, K., Shafiani, S., Ernst, J., 2011. Initiation and regulation of T-cell responses in  
514 tuberculosis. *Mucosal Immunol.* 4, 288–293. <https://doi.org/10.1038/mi.2011.10>  
515
- 516 Vivier, E., Artis, D., Colonna, M., Diefenbach, A., Santo, J.P.D., Eberl, G., Koyasu, S.,  
517 Locksley, R.M., McKenzie, A.N.J., Mebius, R.E., Powrie, F., Spits, H., 2018. Innate  
518 Lymphoid Cells: 10 Years On. *Cell* 174, 1054–1066.  
519 <https://doi.org/10.1016/j.cell.2018.07.017>  
520
- 521 Vivier, E., van de Pavert, S.A., Cooper, M.D., Belz, G.T., 2016. The evolution of innate  
522 lymphoid cells. *Nat. Immunol.* 17, 790–794. <https://doi.org/10.1038/ni.3459>  
523
- 524 Wallrapp, A., Riesenfeld, S.J., Burkett, P.R., Abdunour, R.-E.E., Nyman, J., Dionne,  
525 D., Hofree, M., Cuoco, M.S., Rodman, C., Farouq, D., Haas, B.J., Tickle, T.L.,  
526 Trombetta, J.J., Baral, P., Klose, C.S.N., Mahlaköiv, T., Artis, D., Rozenblatt-Rosen,

527 O., Chiu, I.M., Levy, B.D., Kowalczyk, M.S., Regev, A., Kuchroo, V.K., 2017. The  
528 neuropeptide NMU amplifies ILC2-driven allergic lung inflammation. *Nature* 549, 351–  
529 356. <https://doi.org/10.1038/nature24029>  
530

531 Weizman, O.-E., Adams, N.M., Schuster, I.S., Krishna, C., Pritykin, Y., Lau, C., Degli-  
532 Esposti, M.A., Leslie, C.S., Sun, J.C., O’Sullivan, T.E., 2017. ILC1 Confer Early Host  
533 Protection at Initial Sites of Viral Infection. *Cell* 171, 795-808.e12.  
534 <https://doi.org/10.1016/j.cell.2017.09.052>  
535

536 Zeis, P., Lian, M., Fan, X., Herman, J.S., Hernandez, D.C., Gentek, R., Elias, S.,  
537 Symowski, C., Knöpper, K., Peltokangas, N., Friedrich, C., Doucet-Ladeveze, R.,  
538 Kabat, A.M., Locksley, R.M., Voehringer, D., Bajenoff, M., Rudensky, A.Y.,  
539 Romagnani, C., Grün, D., Gasteiger, G., 2020. In Situ Maturation and Tissue  
540 Adaptation of Type 2 Innate Lymphoid Cell Progenitors. *Immunity* 53, 775-792.e9.  
541 <https://doi.org/10.1016/j.immuni.2020.09.002>  
542

## 543 **Materials & Methods**

### 544 **Mice**

545

546 Six-to-eight-week-old female C57BL/6 mice were purchased from Charles River  
547 Laboratories France (Saint Germain Nuelles, France). *Rag2*<sup>-/-</sup> (B6.129-Rag2tm1Fwa),  
548 Red5 mice (B6(C)-Il5tm1.1(icre)Lky/J)n, *Rag2*<sup>-/-</sup>*γc*<sup>-/-</sup> (C;129S4-Rag2tm1.1Flv  
549 Il2rgtm1.1Flv/J) on a C57BL/6 J were bred in our animal facility. ROSA26-YFP mice  
550 (B6.129X1-Gt(ROSA)26Sor<sup>tm1(EYFP)Cos</sup>/J; 006148) were purchased from The Jackson  
551 Laboratory through Charles Rivers Laboratory France. All mice were maintained in  
552 specific-pathogen-free animal facility at IPBS and all experiments were conducted in  
553 strict accordance with French laws and regulations in compliance with the European  
554 Community council directive 68/609/EEC guidelines and its implementation in France  
555 under procedures approved by the French Ministry of Research and the FRBT (C2EA-  
556 01) animal care committee (APAFIS #1269, #3873, #10546, #16529 and #17384).

557

### 558 ***Mtb* culture, immunization & mouse infections**

559

560 The laboratory strain of *Mtb*, H37Rv, was grown at 37°C in Middlebrook 7H9 medium  
561 (Difco) supplemented with 10% albumin-dextrose-catalase (ADC, Difco) and 0.05%  
562 Tyloxapol (Sigma), or on Middlebrook 7H11 agar medium (Difco) supplemented with  
563 10% oleic acid-albumin-dextrose-catalase (OADC, Difco). Six- to eight-week-old mice  
564 were anesthetized with a cocktail of ketamine (60 mg/kg, Merial) and xylazine (10  
565 mg/kg, Bayer) and infected intranasally (i.n.) with 1000 CFUs of mycobacteria in 25 μL  
566 of PBS containing 0.01% Tween 80. For immunization, C57BL/B6 mice were  
567 immunized i.n. with 5.10<sup>5</sup> CFU of BCG (Danish), and were challenged 60 days post-  
568 vaccination with H37Rv as previously described. All experiments using *Mtb* were  
569 performed in appropriate biosafety level 3 (BSL3) laboratory and animal facility.

570

### 571 ***In vivo* treatments**

572

573 2-DG (1g/kg, Sigma) was injected every other day starting from the day of infection  
574 and until completion of the experiment. For glucose supplementation, mice were

575 treated with drinking water containing 30% (w/v) glucose (started 1 week before  
576 infection until sacrifice).

577

### 578 **Adoptive transfer experiments**

579

580 For the adoptive transfer of total lung ILC2, *in vitro* cultured of ILC2 were harvested  
581 after 7 days of culture and  $5 \times 10^5$  to  $2 \times 10^6$  cells were transferred i.v. in mice  
582 anesthetized with isoflurane one day before *Mtb* infection in  $\text{Rag2}^{-/-}\gamma\text{c}^{-/-}$ . For the  
583 adoptive transfer of the  $\text{IL-18R}\alpha^{-}$  or  $\text{IL-18R}\alpha^{+}$  ILC2 subsets, both subsets were FACS-  
584 sorted and cultured *in vitro* for 7 days in complete RPMI supplemented with 10% FBS.  
585 At the end of the culture, cells were harvested and  $1 \cdot 10^5$  cells were transferred i.v. in  
586  $\text{Rag2}^{-/-}\gamma\text{c}^{-/-}$  mice anesthetized with isoflurane, one day before i.n. *Mtb* infection. For  
587 ILC1-like transfer,  $1 \times 10^4$  purified ILC1-like were directly transferred via intratracheal  
588 (i.t.) route in mice anesthetized with isoflurane one day before *Mtb* infection in  $\text{Rag2}^{-/-}$   
589  $\gamma\text{c}^{-/-}$ .

590

### 591 **Lung harvest**

592

593 Mice were sacrificed any cervical dislocation under isoflurane anesthesia and lungs  
594 were harvested aseptically, homogenized using a gentleMACS dissociator (C Tubes,  
595 Miltenyi) in HBSS (Difco), and incubated with DNase I (0.1 mg/mL, Roche) and  
596 collagenase D (2 mg/mL, Roche) during 30 min at 37°C under 5% CO<sub>2</sub>. When  
597 indicated, mice received an i.v. injection of labeled anti-CD45 mAb (5µg) 5 minutes  
598 before sacrifice to discriminate between parenchymal and intravascular cells in  
599 subsequent flow cytometry analyses. Lung homogenates were filtered on 40 µm cell  
600 strainers and centrifuged at  $329 \times g$  during 5 min. Supernatants were conserved for  
601 cytokine content analysis. A part of the cellular pellet was conserved in TRIzol reagent  
602 for cellular RNA analysis. Bacterial loads (colony forming units) were determined by  
603 plating serial dilutions of the lung homogenates onto 7H10 solid medium (Difco)  
604 supplemented with 10% oleic acid-albumin-dextrose-catalase (OADC, Difco). The  
605 plates were incubated at 37°C for 3 weeks before bacterial CFUs scoring. In the  
606 remaining fraction, red blood cells were lysed in 150 mM NH<sub>4</sub>Cl, 10 mM KHCO<sub>3</sub>, 0.1  
607 mM EDTA (pH 7.2) for immunological staining.

608

## 609 ***In situ* expansion of ILC**

610

611 To expand ILC2, C57BL/6 or *Rag2*<sup>-/-</sup> mice were treated intranasally (i.n.) with 100 ng  
612 of recombinant IL-33 (Biolegend) each day for 5 consecutive days. For the cytokine-  
613 based plasticity model, C57BL/6 or *Rag2*<sup>-/-</sup> mice were treated i.n. with different  
614 combinations of cytokines specified in figures legends at day 1, 3, 5, 8 and sacrificed  
615 at day 9: 100 ng of IL-12 (R&D), IL-18 (R&D), IL-33 (Biolegend) or 20 µg of NMU (US  
616 Biological) per mouse and per instillation. For the Seahorse assays we elicited ILC2  
617 with 0.5 mg IL-33, three doses i.p. over 10 days. Sorted ILC2 from lung were then  
618 cultured in presence of IL-7 and IL-2 (50ng/ml) for 7 days before addition of DMOG.

619

## 620 **Flow cytometry**

621

622 To identify mouse ILCs, single-cell suspensions were stained with mAb for known  
623 lineages and with mAb discriminating ILC subsets. mAbs for known lineages included  
624 CD3 (17A2, Biolegend), CD4 (RM4-5, Biolegend), CD8a (53-6.7, Biolegend), TCRαβ  
625 (H57-597, Biolegend), TCRγδ, (GL3, Biolegend) CD11b (M1/70, Biolegend), CD11c  
626 (N418, Biolegend), F4/80 (BM8, Biolegend), Ly6G (1A8, Biolegend), TER119 (TER-  
627 119, Biolegend), FcεR1a (MAR-1, Biolegend), CD19 (1D3/CD19, Biolegend), B220  
628 (RA3-6B2, Biolegend), and CD49b (DX5, Biolegend). mAbs discriminating ILC subsets  
629 included CD45.2 (104, BD), CD90.2 (30-H12, Biolegend), CD127 (A7R34,  
630 eBioscience), NK1.1 (PK136, BD Biosciences), IL-18Rα (P3TUNYA, eBioscience),  
631 ST2 (RMST2-2, eBioscience), CD226 (10E5, Biolegend), and CD49a (Ha31/8), NKp46  
632 (29A1.4). mAbs for intracellular staining included GATA3 (L50-823, BD Biosciences),  
633 T-bet (4B10, eBiosciences), RORγt (Q31-378, BD Biosciences), TCF-1 (S33-966, BD),  
634 Arg1 (A1exF5, BD Biosciences), Ki-67 (SolA15, eBiosciences), Eomes (Dan11mag,  
635 eBiosciences), and HIF1α (D1S7W, Cell Signaling). After extracellular staining, cells  
636 were fixed and permeabilized (Foxp3 staining kit, eBiosciences) for intracellular  
637 staining. Samples from Biosafety Level 3 were inactivated for 2 hours at RT with 4%  
638 paraformaldehyde (ThermoFisher Scientific) after extracellular and intracellular  
639 staining.

640 Live/Dead fixable blue (eBiosciences) and mouse FcBlock (BD Biosciences) were  
641 used for all flow cytometry experiments. Cell staining was analyzed using LSR

642 Fortessa flow cytometers (BD) and FlowJo software (v10). Cells were first gated in  
643 singlets (FSC-H vs. FSC-W and SSC-H vs. SSC-W) and live cells before further  
644 analyses.

645

### 646 **Intracellular cytokines staining**

647

648 For intracellular cytokines staining of ILCs, single-cell suspensions from lung were  
649 incubated at 37°C with Brefeldin A in association or not with PMA (50 ng/ml,  
650 Sigma)/Ionomycine (500 ng/ml, Sigma) or 50 ng/ml of IL-12 and IL-18 for 4 hours  
651 before being surface stained, fixed and permeabilized (Foxp3 staining kit,  
652 eBiosciences). mAbs for cytokines staining included IFN- $\gamma$  (XMG1.2, Biolegend), IL-  
653 17A (TC11-18H10, BD Biosciences), IL-5 (TRFK5, BD Biosciences), and IL-13  
654 (eBio13A, eBiosciences) For HIF1 $\alpha$  staining of ILCs, single-cell suspensions from lung  
655 were incubated at 37°C with DMOG (500 $\mu$ M) for 3 hours before being surface stained,  
656 fixed and permeabilized (Foxp3 staining kit, eBiosciences). In order to block glycolysis  
657 during *ex vivo* stimulation, cells were incubated in the presence of 10mM 2-DG  
658 (Sigma). *Mtb* was inactivated by incubation in PFA 4% for 2 hours at room temperature.

659

### 660 **ILC enrichment and cell-sorting**

661

662 Lung ILCs were enriched from lung single-cell suspensions by using the EasySep™  
663 Mouse ILC2 Enrichment Kit (StemCell). After enrichment, cells were stained with  
664 lineage mAb (CD3, CD4, CD8 $\alpha$ , TCR $\alpha\beta$ , TCR $\gamma\delta$ , CD19, B220, CD11b, CD11c, F4/80,  
665 TER119, Fc $\epsilon$ RIa, CD49b, Ly6G) and ILC markers (CD90.2, CD45.2, NK1.1, ST2, IL-  
666 18R $\alpha$ , CD49a). ILC2 were purified as Lin<sup>-</sup>CD45.2<sup>+</sup>CD90.2<sup>+</sup>NK1.1<sup>-</sup>ST2<sup>+</sup>IL-18R $\alpha$ <sup>+/-</sup> ILC1-  
667 like were purified as Lin<sup>-</sup>CD45.2<sup>+</sup>CD90.2<sup>+</sup>NK1.1<sup>-</sup>ST2<sup>-</sup>CD49a<sup>+</sup>IL-18R $\alpha$ <sup>+</sup>. Cells were  
668 sorted using a FACSAria Fusion cytometer (BD, France).

669

### 670 ***In vitro* culture of ILC2**

671

672 Cell sorted ILC2 were incubated in 6-well plates at a density of 300,000 cells per ml  
673 for 4 days with IL-2 (25 ng/ml, R&D) and IL-7 (25 ng/ml, R&D) in RPMI (Difco)  
674 supplemented with 10 % FBS. After 4 days of culture, ILC2 were harvested for adoptive

675 transfer or incubated with DMOG (Sigma). For DMOG experiment, half of the medium  
676 was removed and replaced with fresh medium containing IL-2 (25 ng/ml) and IL-7 (25  
677 ng/ml) with or without DMOG (500  $\mu$ M) for 3 more days. Cell sorted ILC2 were  
678 incubated in 6-well plates at a density of 300,000 cells per ml for 4 days with IL-2 (25  
679 ng/ml, R&D) and IL-7 (25 ng/ml, R&D) in RPMI (Difco) supplemented with 10 % FBS.  
680 After 4 days of culture, ILC2 were harvested for adoptive transfer or incubated with  
681 DMOG (Sigma). For DMOG experiment, half of the medium was removed and  
682 replaced with fresh medium containing IL-2 (25 ng/ml) and IL-7 (25 ng/ml) with or  
683 without DMOG (500  $\mu$ g/ml) for 3 more days. For the Seahorse assays, sorted ILC2  
684 from lung were cultured in presence of IL-7 and IL-2 (50ng/ml) for 7 days before  
685 addition of DMOG.

686

### 687 **SCENITH assay**

688

689 SCENITH experiments were performed as previously described (Argüello et al., 2020)  
690 using the SCENITH kit containing all reagents and anti-puromycin antibodies  
691 (requested from [www.scenith.com/try-it](http://www.scenith.com/try-it)). Briefly, lung cell suspensions were  
692 stimulated for 15 minutes at 37°C in the presence of the indicated inhibitors of various  
693 metabolic pathways then incubated for 30 minutes with puromycin at 37°C. At the end  
694 of the incubation, puromycin was stained with fluorescent anti-puromycin antibodies  
695 (Clone R4743L-E8) by flow cytometry and the impact of the various metabolic inhibitors  
696 was quantitated as described (Argüello et al., 2020).

697

### 698 **Seahorse experiments**

699

700 1.5 to 2  $\times 10^5$  FACS sorted lung ILC2s per well were rested in a 96-well plate in  
701 Glutamax RPMI (supplemented with 10% fetal bovine serum, non-essential amino  
702 acids, 1 mM sodium pyruvate, 85  $\mu$ M 2-mercapto-ethanol and 100 U/ml penicillin-  
703 streptomycin) containing 25 ng/ml IL-7. After 24h cells were split and rested in fresh  
704 IL-7 containing media for another 3 days. Subsequently, cells were cultured in fresh  
705 medium containing 25 ng/ml IL-7 and 20 ng/ml of IL-2 in the presence or absence of  
706 0.5 mM DMOG for a further 72 hours. To prepare for extracellular flux analysis cells  
707 were then washed thoroughly in XF medium (modified DMEM) and adhered to the  
708 Seahorse plate using 22.4  $\mu$ g/ml Cell-Tak (Corning).



709 For glycolytic stress test, cells were plated at a density of  $2 \times 10^5$  cells/well in XF medium  
710 supplemented with 2 mM glutamine. Cells were incubated for 30-60 min at 37°C and  
711 ECAR was measured under basal conditions, and in response to 10 mM glucose, 2  
712  $\mu$ M oligomycin and 50 mM 2-DG. For the mitochondrial stress test, cells were plated  
713 at a density of  $1.5 \times 10^5$  cells/well in XF medium supplemented with 2 mM glutamine, 1  
714 mM sodium pyruvate and 25 mM glucose. Cells were incubated for 30-60 min at 37°C.  
715 OCAR was measured under basal conditions, after injection of 2  $\mu$ M oligomycin, 1.5  
716  $\mu$ M FCCP and 100 nM rotenone + 1  $\mu$ M antimycin A. Extracellular flux assays were  
717 done using a 96-well extracellular flux analyzer XFe-96 (Seahorse Bioscience).

718 Normalization by protein was used to correct for potential differences in seeding  
719 densities across wells. Protein measurement was performed using the Pierce BCA  
720 protein assay according to the manufacturer instructions.

#### 721 **Quantitative RT-PCR analysis of transcripts**

722

723 RNA from lungs homogenates was extracted using TRIzol reagent (Ambion) and  
724 RNeasy spin columns according to manufacturer's instructions (RNeasy kit, Qiagen).  
725 RNA was reverse transcribed into cDNA using M-MLV Reverse transcriptase  
726 (Invitrogen). RT-qPCR was performed using gene-targeted primers (Supplementary  
727 Table 1) as described above. Values were normalized using the housekeeping beta-  
728 actin gene (*Actb*) and expressed as a fold change. RNA from ILC2 culture were  
729 extracted using RLT (Qiagen) and RNA were reverse transcribed as previously  
730 described (Troegeler et al., 2017).

731

#### 732 **Statistical analyses**

733

734 Statistical analyses were performed using GraphPad Prism 9 software. Agostino and  
735 Pearson normality tests were performed to determine whether data followed a normal  
736 distribution. Unpaired *t*-test (for normal data) or Mann-Whitney (for non-normal data)  
737 were performed when two samples were compared; ANOVA (for normal data) or  
738 Kruskal-Wallis (for non-normal data) tests were performed when more than two  
739 samples were compared. For all analyses, \* indicates  $P < 0.05$ , \*\* indicates  $P < 0.01$ ,  
740 \*\*\* indicates  $P < 0.001$ , and \*\*\*\* indicates  $P < 0.0001$ .

741

## 742 **Acknowledgements**

743

744 We thank Yasmine Belkaid (NIH/NIAID, Bethesda) for critical review of the manuscript.  
745 We acknowledge Emmanuelle Näser (Genotoul TRI-IPBS platform, Toulouse) for flow  
746 cytometry and cell-sorting, Flavie Moreau, Céline Berrone and Aline Tridon (Genotoul  
747 Anexplor-IPBS platform, Toulouse), and Sylvie Appolinaire and Celine Berraud  
748 (CREFRE US006, Toulouse) for mouse care and maintenance in conventional and  
749 BSL3 facilities. We thank Richard Locksley (USCF, San Francisco) for the kind gift of  
750 Red5 mice. We thank Geanncarlo Lugo-Villarino, Sophie Laffont (CPTP, Toulouse)  
751 and Andrea Pichler (CRCT, Toulouse) for helpful discussions. This work was  
752 supported by Centre de la Recherche Scientifique (CNRS), the University Toulouse  
753 III-Paul Sabatier, the French Ministry for Higher Education, Research and Innovation  
754 (fellowship to D.C.), the Fondation pour la Recherche Médicale (grant  
755 DEQ20160334902 to O.N.), the Bettencourt Schueller Foundation (grants Coup d'Élan  
756 pour la recherche française and Explore-TB to O.N.), MSDAVENIR (grant Fight-TB to  
757 O.N.), the Agence Nationale de la Recherche (grants ANR-18-CE15-0004-01 to D.H.  
758 and ANR-11-EQUIPEX-0003 to O.N.), and the European Commission (grant  
759 TBVAC2020 n°643381 to O.N.). M.R.H. is supported by a Royal Society and Wellcome  
760 Trust Sir Henry Dale fellowship (105644/Z/14/Z), a Lister Institute of Preventative  
761 Medicine Prize and a BBSRC Project grant (BB/T014482/1). The funders had no role in  
762 study design, data collection, and analysis, decision to publish, or preparation of the  
763 manuscript.

764

## 765 **Author contributions**

766

767 D.C. and D.H. conceived and designed the study with input from O.N.; D.C., A.C.,  
768 M.Z.K., E.B., T.S. and F.L. performed the experiments; E.L., J-P.G., and R.J.A  
769 contributed critical reagents and methods, D.C., G.E., J-C.G., R.J.A., M.R.H. and D.H.  
770 analyzed and interpreted the data; J-C.G., G.E., M.R.H., and Y.P., also provide  
771 important discussion for the project and critical feedback on the manuscript; D.C., O.N.  
772 and D.H. wrote the manuscript. All coauthors read, reviewed and approved the  
773 manuscript.

774

## 775 **Competing interests**

776

777 The authors declare no competing interests

778

## Figure legends

779

780 **Figure 1. IL-18R $\alpha$ -expressing ILC2 differentiate into ILC1-like cells during *Mtb***  
781 **infection (A)** Representative dot plots showing the gating strategy used to analyze  
782 ILC subsets in the lungs of C57BL/6 mice after doublets exclusion (top graphs): ILC1  
783 (dark blue), ILC3 (red), IL-18R $\alpha$ <sup>-</sup> ILC2 (green), IL-18R $\alpha$ <sup>+</sup> ILC2 (yellow) and T-bet<sup>+</sup>IL-  
784 18R $\alpha$ <sup>+</sup> ILC (light blue) are depicted in non-infected and *Mtb*-infected mice. **(B)**  
785 Unsupervised t-SNE distribution of total lung Lin<sup>-</sup>CD90.2<sup>+</sup> populations at steady-state  
786 (left graph) and during *Mtb* infection (right graph). Based on gating strategy defined in  
787 Figure 1A, ILC subsets were depicted with the same color code: ILC1 in dark blue,  
788 ILC3 in red, IL-18R $\alpha$ <sup>-</sup> ILC2 in green, IL-18R $\alpha$ <sup>+</sup> ILC2 in yellow and ILC1-like cells (light  
789 blue). **(C)** Expression of GATA3 (MFI), ST2 (%), and Arg1 (%) in indicated ILC subsets  
790 at day 28 post-infection in C57BL/6 mice. **(D)** Expression of T-bet (MFI), CD49a (%)  
791 and CD226 (MFI) in indicated ILC subsets at day 28 post-infection in C57BL/6 mice.  
792 **(E)** Percentages of IFN- $\gamma$ , IL-5, and IL-17A positive cells in the indicated ILC subsets  
793 after *ex vivo* stimulation with PMA/ionomycin in presence of Brefeldin A for 4h at day  
794 28 post-infection in C57BL/6 mice. **(F)** Absolute numbers of ILC1-like cells at the  
795 indicated days after *Mtb* infection. Prior to sacrifice, mice were injected with fluorescent  
796 anti-CD45.2 to distinguish vascular and parenchymal cells. ILC1-like cells have been  
797 gated on lung-resident cells. **(G)** Percentages of IFN- $\gamma$ <sup>+</sup> cells in the indicated ILC  
798 subsets after *ex vivo* stimulation with IL-12+IL-18 or not, in presence of Brefeldin A for  
799 4h at day 28 post-infection in C57BL/6 mice. **(H)** Absolute numbers of IL-18R $\alpha$ <sup>+</sup> ILC2  
800 at the indicated days after *Mtb* infection. Prior to sacrifice, mice were injected with  
801 fluorescent anti-CD45.2 to distinguish vascular and parenchymal cells. IL-18R $\alpha$ <sup>+</sup> ILC2  
802 have been gated on lung-resident cells. **(I)** Experimental settings for the adoptive  
803 transfer of IL-18R $\alpha$ <sup>-</sup> and IL-18R $\alpha$ <sup>+</sup> ILC2 into Rag2<sup>-/-</sup> $\gamma$ c<sup>-/-</sup> before *Mtb* infection. **(J)**  
804 Percentage of ILC (Lin<sup>-</sup>CD45.2<sup>+</sup>CD90.2<sup>+</sup>CD127<sup>+</sup>) in lung at day 21 post-infection in  
805 Rag2<sup>-/-</sup> $\gamma$ c<sup>-/-</sup> after adoptive transfer of IL-18R $\alpha$ <sup>-</sup> ILC2 (green) and IL-18R $\alpha$ <sup>+</sup> ILC2 (yellow).  
806 **(K)** As in **(J)**, but for T-bet expression in ILC. In **(C, D, F and H)**, data are representative  
807 of five independent experiments, in **(E, G)** data are representative of two independent  
808 experiments and in **(J, K)** data are a pool of two independent experiments with each  
809 symbol representing an individual mouse, graphs depict data as mean ( $\pm$  s.e.m) and

810 statistical analysis was performed using two-way **(E-F)**, one-way ANOVA **(C-D, G-H)**  
811 **or** Mann Whitney test **(J-K)** (\*,  $p < 0.05$ ; \*\*,  $P < 0.01$ ; \*\*\*,  $p < 0.001$ ; \*\*\*\*,  $p < 0.0001$ ).

812 **Figure 2. The inflammatory environment shapes the fate of IL-18R $\alpha$ <sup>+</sup> ILC2. (A)**  
813 Representative dot-plots of T-bet and IL18R $\alpha$  expression after intranasal  
814 administration of PBS and IL-12+IL-18 in *Rag2*<sup>-/-</sup> mice in Lin<sup>-</sup>CD45.2<sup>+</sup>CD90.2<sup>+</sup>NK1.1<sup>-</sup>  
815 ROR $\gamma$ <sup>t</sup> cells **(B)** Absolute numbers of IL-18R $\alpha$ <sup>-</sup> ILC2 (green), IL-18R $\alpha$ <sup>+</sup> ILC2 (yellow)  
816 and ILC1-like cells (blue) after cytokine (IL-12+IL-18) or control (PBS) treatment. **(C)**  
817 Percentage of TCF-1 in lung IL-18R $\alpha$ <sup>-</sup> ILC2 after intranasal administration of PBS  
818 (white dots) or IL-12+IL-18 (grey dots). **(D)** Percentages of cells expressing IL-5 or IFN- $\gamma$   
819  $\gamma$  among the indicated ILC subsets after *ex vivo* stimulation with PMA/ionomycin in the  
820 presence of brefeldin A for 4h. **(E)** Percentages of IFN- $\gamma$ <sup>+</sup> cells in the indicated ILC  
821 subsets after *ex vivo* stimulation with IL-12+IL-18, PMA/ionomycin or not in presence  
822 of Brefeldin A for 4h from IL-12+IL-18 treated C57BL/6 mice. **(F)** Representative dot-  
823 plots of T-bet and IL18R $\alpha$  expression after intranasal administration of IL-33, IL-12+IL-  
824 18 and IL-12+IL-18+IL-33 in *Rag2*<sup>-/-</sup> mice in Lin<sup>-</sup>CD45.2<sup>+</sup>CD90.2<sup>+</sup>NK1.1<sup>-</sup>ROR $\gamma$ <sup>t</sup> cells.  
825 **(G-I)** Absolute numbers of IL-18R $\alpha$ <sup>-</sup> ILC2 **(G)**, IL-18R $\alpha$ <sup>+</sup> ILC2 **(H)** and ILC1-like cells **(I)**  
826 after intranasal administration of IL-33, IL-12+IL-18, or IL-12+IL-18+IL-33. **(J)**  
827 Expression of ST2 (%), Arg1 (%) and CD49a (%) in IL-18R $\alpha$ <sup>+</sup> ILC2 in IL-33 (black  
828 dots), IL-12+IL-18 (white dots) and IL-12+IL-18+IL-33 (grey dots) -treated mice. **(K)**  
829 Percentage of IL-5<sup>+</sup>IFN- $\gamma$ <sup>-</sup> (right), IL-5<sup>-</sup>IFN- $\gamma$ <sup>+</sup> (middle), IL-5<sup>+</sup>IFN- $\gamma$ <sup>+</sup> (left) in IL-18R $\alpha$ <sup>+</sup>  
830 ILC2 in IL-33 (black dots), IL-12+IL-18 (white dots) and IL-12+IL-18+IL-33 (grey dots)  
831 -treated mice. **(L)** Absolute numbers of IL-18R $\alpha$ <sup>+</sup> ILC2 (left) and ILC1-like cells (right)  
832 after intranasal administration of PBS (control), neuromedin U (NMU), IL-12+IL-18, or  
833 IL-12+IL-18+NMU. Each symbol represents an individual mouse. Statistical analysis  
834 was performed using Mann-Whitney **(B, C)**, one-way **(G-K)** and two-way **(D-E, L)**  
835 ANOVA tests (\*, p<0.05; \*\*, P<0.01; \*\*\*, p<0.001; \*\*\*\*, p<0.0001). Graphs depict data  
836 as mean ( $\pm$  s.e.m). Data are representative of three **(B, D, G-K)**, and two **(C, E, L)**  
837 independent experiments.

838

839

840

841 **Figure 3. Metabolic reprogramming toward glycolysis is associated with an ILC1-**  
842 **like cell differentiation. (A)** Representative histograms of puromycin staining in NK  
843 cells (violet), IL-18R $\alpha$ <sup>-</sup> ILC2 (green), IL-18R $\alpha$ <sup>+</sup> ILC2 (yellow), and ILC1-like cells (blue)  
844 in IL-12+IL-18-treated mice. **(B)** Expression of puromycin (MFI) in NK cells (violet), IL-  
845 18R $\alpha$ <sup>-</sup> ILC2 (green), IL-18R $\alpha$ <sup>+</sup> ILC2 (yellow), and ILC1-like cells (blue) in PBS vs. IL-  
846 12+IL-18 treated mice. **(C)** Percentages of puromycin-positive cells in NK cells (violet),  
847 IL-18R $\alpha$ <sup>-</sup> ILC2 (green), IL-18R $\alpha$ <sup>+</sup> ILC2 (yellow), and ILC1-like cells (blue) in PBS vs.  
848 IL-12+IL-18 treated mice. **(D)** Representative histograms of puromycin staining (left)  
849 and quantification (MFI, right) in ILC1-like cells from IL-12+IL-18 treated mice after  
850 incubation with various metabolic inhibitors (Co, control; DG, 2-Deoxyglycose; O,  
851 oligomycin; DGO, 2-Deoxyglucose + Oligomycin). **(E-F)** Percentages of mitochondrial  
852 dependence **(E)**, and glycolytic capacity **(F)** in NK (violet), IL-18R $\alpha$ <sup>-</sup> ILC2 (green), IL-  
853 18R $\alpha$ <sup>+</sup> ILC2 (yellow), and ILC1-like cells (blue) in PBS vs. IL-12+IL-18 treated mice.  
854 **(G)** Percentages of Arg1<sup>+</sup> cells among IL-18R $\alpha$ <sup>-</sup> ILC2 (green), IL-18R $\alpha$ <sup>+</sup> ILC2 (yellow),  
855 and ILC1-like cells (blue) defined after intranasal administration of PBS (control) or  
856 cytokines (IL-12+IL-18). **(H)** Histograms showing HIF1 $\alpha$  expression in IL-18R $\alpha$ <sup>-</sup> ILC2  
857 (left), IL-18R $\alpha$ <sup>+</sup> ILC2 (middle) and ILC1-like cells in PBS (black line) or IL-12+IL-18  
858 (blue line) treated mice. Dash line represents isotype control for HIF1 $\alpha$  staining. Due  
859 to the absence of ILC1-like cells at steady-state, only the condition with IL-12+IL-18  
860 treatment is represented. **(I)** Histograms showing HIF1 $\alpha$  protein expression in ILC2  
861 cultured in the absence (vehicle, grey) or presence of DMOG (blue). The dot line  
862 represents FMO for HIF1 $\alpha$  detection. **(J-L)** Quantitative analysis of the intensity  
863 of GATA3 **(J)**, ST2 **(K)** and IL-5 **(L)** expression in ILC2 cultured in the absence (vehicle)  
864 or presence of DMOG. **(M)** Seahorse analysis of glycolytic stress test with  
865 quantification of glycolysis and glycolytic capacity of ILC2 cultured in the presence or  
866 absence of DMOG. **(N)** Seahorse analysis of mitochondrial respiration with  
867 quantification of spare respiratory capacity of ILC2 cultured in the presence or absence  
868 of DMOG. **(O)** as in **(J-L)** except that the expression of *Tbx21*, *Ifng* and *Il18ra1* mRNA  
869 was analyzed by RT-qPCR. Each symbol represents an individual mouse and  
870 statistical analysis was performed using two-way ANOVA **(B, C, E, F, G)**, and paired t  
871 test **(J-O)** (\*, p<0.05; \*\*, P<0.01; \*\*\*, p<0.001; \*\*\*\*, p<0.0001). Graphs depict data as  
872 mean ( $\pm$  s.e.m) from two **(A-N)** and a pool of three **(O)** independent experiments.

873 **Figure 4. ILC1-like cells confer protection against *Mtb*.** (A) C57BL/6 were  
874 vaccinated by intranasal administration of BCG or not (PBS) 60 days before infection.  
875 After 14 days post-infection, mice were euthanized. (B) Mycobacterial loads at day 14  
876 post-infection in C57BL/6 mice vaccinated or not (PBS) with  $1 \times 10^5$  BCG via the  
877 intranasal route 60 days prior *Mtb* infection. (C) Percentages of total lung ILC  
878 expressing T-bet. (D) Absolute numbers of ILC1 (dark blue), ILC3 (red), IL-18R $\alpha^-$  ILC2  
879 (green), IL-18R $\alpha^+$  ILC2 (yellow) and ILC1-like cells (light blue) at day 14 post-infection  
880 in C57BL/6 mice vaccinated or not (PBS) with  $1 \times 10^5$  BCG via the intranasal route 60  
881 days prior *Mtb* infection. (E) Percentages of IFN- $\gamma^+$  cells among ILC1-like cells in *Mtb*-  
882 infected unvaccinated vs. vaccinated mice after *ex vivo* stimulation with IL-12+IL-18 in  
883 the presence of brefeldin A for 4h. (F) Schematic representation of the *in vivo*  
884 expansion of ILC1-like cells in *Rag2<sup>-/-</sup>* mice treated with IL-12+IL-18+IL-33, cell-sorting  
885 of ILC1-like cells (Lin $^-$ CD45.2 $^+$ CD90.2 $^+$ NK1.1 $^-$ ST2 $^-$ CD49a $^+$ IL-18R $\alpha^+$ ) and adoptive  
886 transfer in *Rag2<sup>-/-</sup>Il2rg<sup>-/-</sup>* one day before infection with *Mtb* by intratracheal route. (G)  
887 Representative histograms of T-bet, GATA3 and ROR $\gamma$ t expression in sorted ILC1-like  
888 cells (grey) vs. ILC2 (Lin $^-$ CD45.2 $^+$ CD90.2 $^+$ NK1.1 $^-$ ST2 $^+$  cells). (H) Bacterial loads at day  
889 21 post-infection in *Rag2<sup>-/-</sup>Il2rg<sup>-/-</sup>* mice having received (+ILC1-like) or not (-ILC1like)  
890 an adoptive transfer of ILC1-like cells from IL-12+IL-18+IL-33 treated *Rag2<sup>-/-</sup>* mice one  
891 day before *Mtb* infection. Each symbol represents an individual mouse. Statistical  
892 analysis was performed using Mann-Whitney test (B-H) (\*,  $p < 0.05$ ; \*\*,  $P < 0.01$ ; \*\*\*,  
893  $p < 0.001$ ; \*\*\*\*,  $p < 0.0001$ ). Graphs depict data as mean ( $\pm$  s.e.m). Data are  
894 representative of two (B-H) independent experiments.

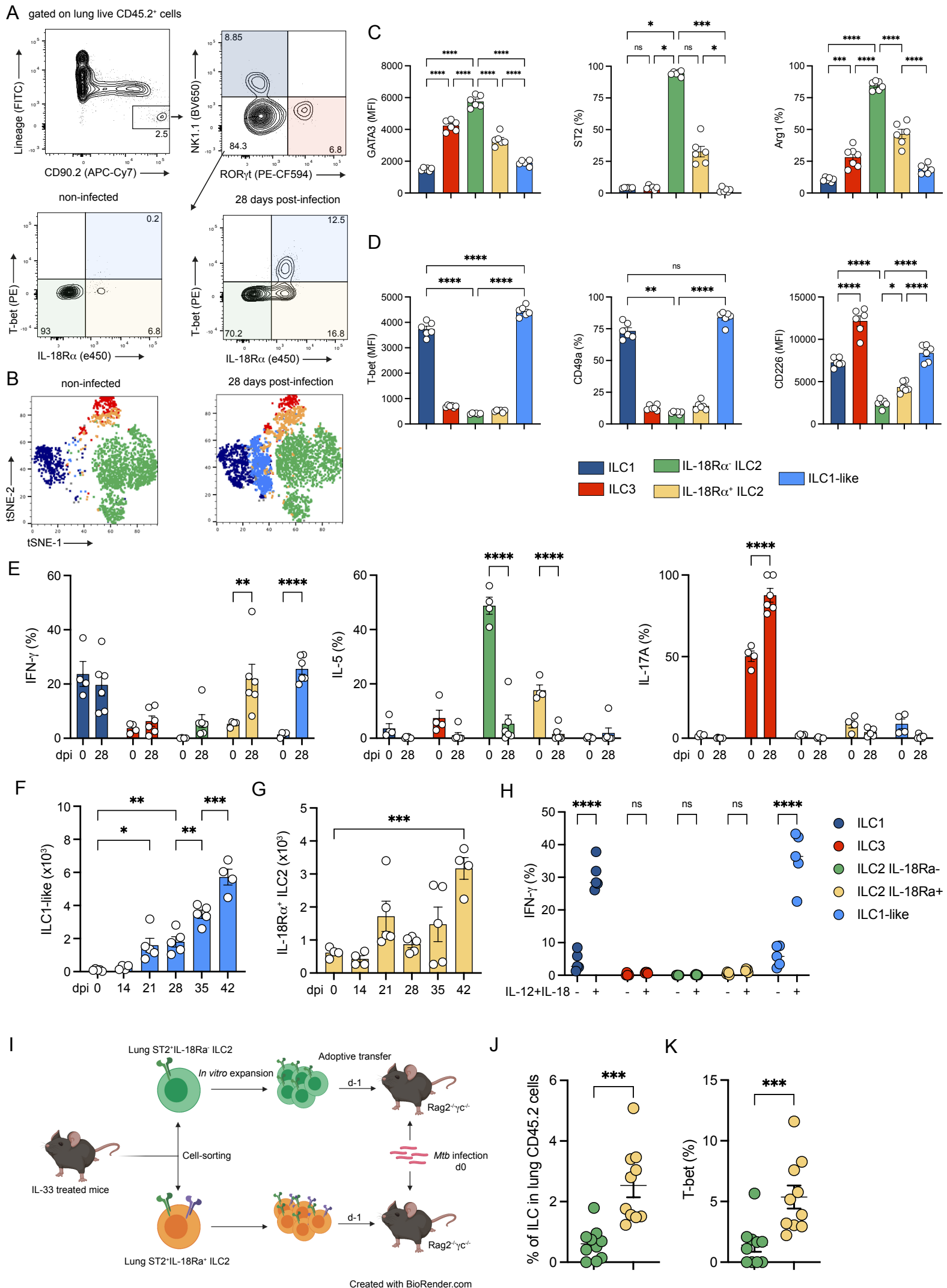


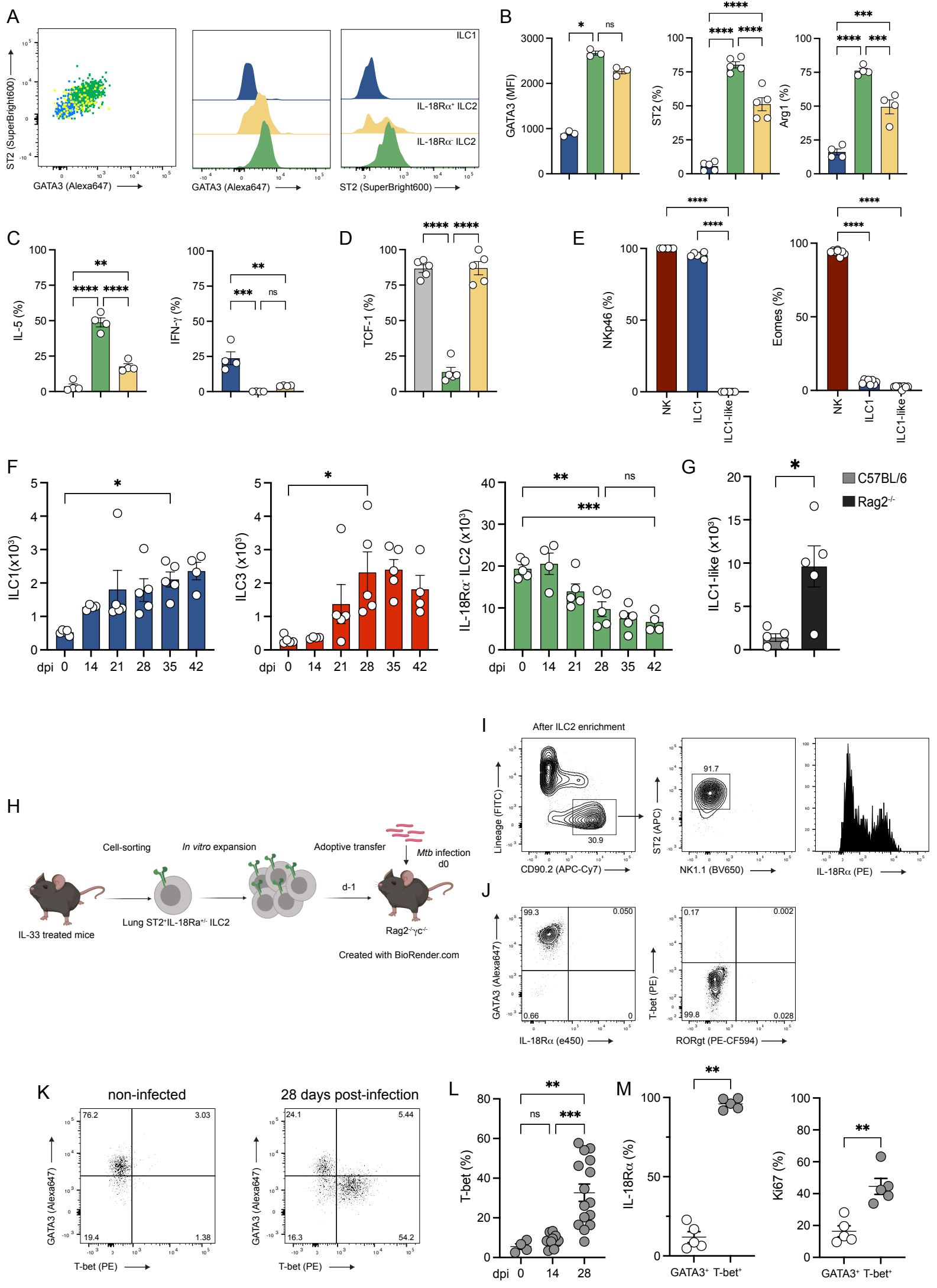
895 **Supplementary Figure 1. Dynamics of ILCs during *Mtb* infection in the mouse**  
896 **model. (A)** Representative expression of GATA3 and ST2 on the indicated ILC  
897 subsets. **(B)** Expression of GATA3 (MFI), ST2 (%) and Arg1 (%) in ILC1 (blue), IL-  
898 18R $\alpha$ <sup>-</sup> ILC2 (green) and IL-18R $\alpha$ <sup>+</sup> ILC2 (yellow) at steady-state in the lung of C57BL/6  
899 mice. **(C)** Expression of IL-5 (%) and IFN- $\gamma$  (%) in the indicated ILC subsets after *ex*  
900 *vivo* stimulation with PMA/ionomycin in presence of Brefeldin A for 4h at steady-state  
901 in the lung of C57BL/6 mice **(D)** Percentages of TCF-1<sup>+</sup> cells in ILC2P from bone  
902 marrow (grey) compared to IL-18R $\alpha$ <sup>-</sup> ILC2 (green) and IL-18R $\alpha$ <sup>+</sup> ILC2 (yellow) from  
903 the lungs of C57BL/6 mice at steady-state. **(E)** Percentages of NKp46<sup>+</sup> (left) and  
904 Eomes<sup>+</sup> (right) cells in ILC1-like cells compared to in NK cells and ILC1 at day 28 post-  
905 infection. **(F)** Absolute numbers of ILC1 (dark blue), ILC3 (red) and IL-18R $\alpha$ <sup>-</sup> ILC2 at  
906 the indicated days after *Mtb* infection. Prior to sacrifice, mice were injected with  
907 fluorescent anti-CD45.2 to distinguish vascular and parenchymal cells. ILC1, ILC3, IL-  
908 18R $\alpha$ <sup>-</sup> ILC2 and IL-18R $\alpha$ <sup>+</sup> ILC2 have been gated on lung-resident cells. **(G)** Absolute  
909 number of ILC1-like cells at day 28 post-infection in C57BL/5 (grey) vs. Rag2<sup>-/-</sup> (black)  
910 mice. **(H)** Schematic representation of the *in vivo* expansion of ILC2 in C57BL/6 or  
911 Rag2<sup>-/-</sup> mice treated with IL-33, cell-sorting, *in vitro* culture and adoptive transfer of  
912 ILC2 in Rag2<sup>-/-</sup>Il2rg<sup>-/-</sup> one day before infection with *Mtb*. **(I)** Gating strategy to purify  
913 ILC2 based on the expression of ST2 (left two graphs) and purity of ILC2 after cell-  
914 sorting (right). **(J)** Phenotype of ILC2 after *in vitro* culture and before adoptive transfer.  
915 **(K)** A representative dot-plot of GATA3 and T-bet expression in Lin<sup>-</sup>CD45.2<sup>+</sup>CD90.2<sup>+</sup>  
916 cells isolated from Rag2<sup>-/-</sup>Il2rg<sup>-/-</sup> mice adoptively transferred with purified ILC2 then left  
917 uninfected (right) or infected with *Mtb* (left). **(L)** Percentages of T-bet expressing ILC  
918 at different days post-infection. **(M)** Expression of IL-18R $\alpha$  (%) and Ki67 (%) in  
919 transferred GATA3<sup>+</sup> (white dots) vs. T-bet<sup>+</sup> (grey dots) ILC at day 28 post-infection in  
920 Rag2<sup>-/-</sup>Il2rg<sup>-/-</sup> mice. Each symbol represents an individual mouse. Statistical analysis  
921 was performed using one-way ANOVA test **(B-F, L)** or Mann-Whitney test **(G, M)** (\*,   
922 p<0.05; \*\*, P<0.01; \*\*\*, p<0.001; \*\*\*\*, p<0.0001). Graphs depict data as mean ( $\pm$   
923 s.e.m). Data are representative of five **(F)**, three **(B-C, K-M)** and two **(D, E, G)**  
924 independent experiments.

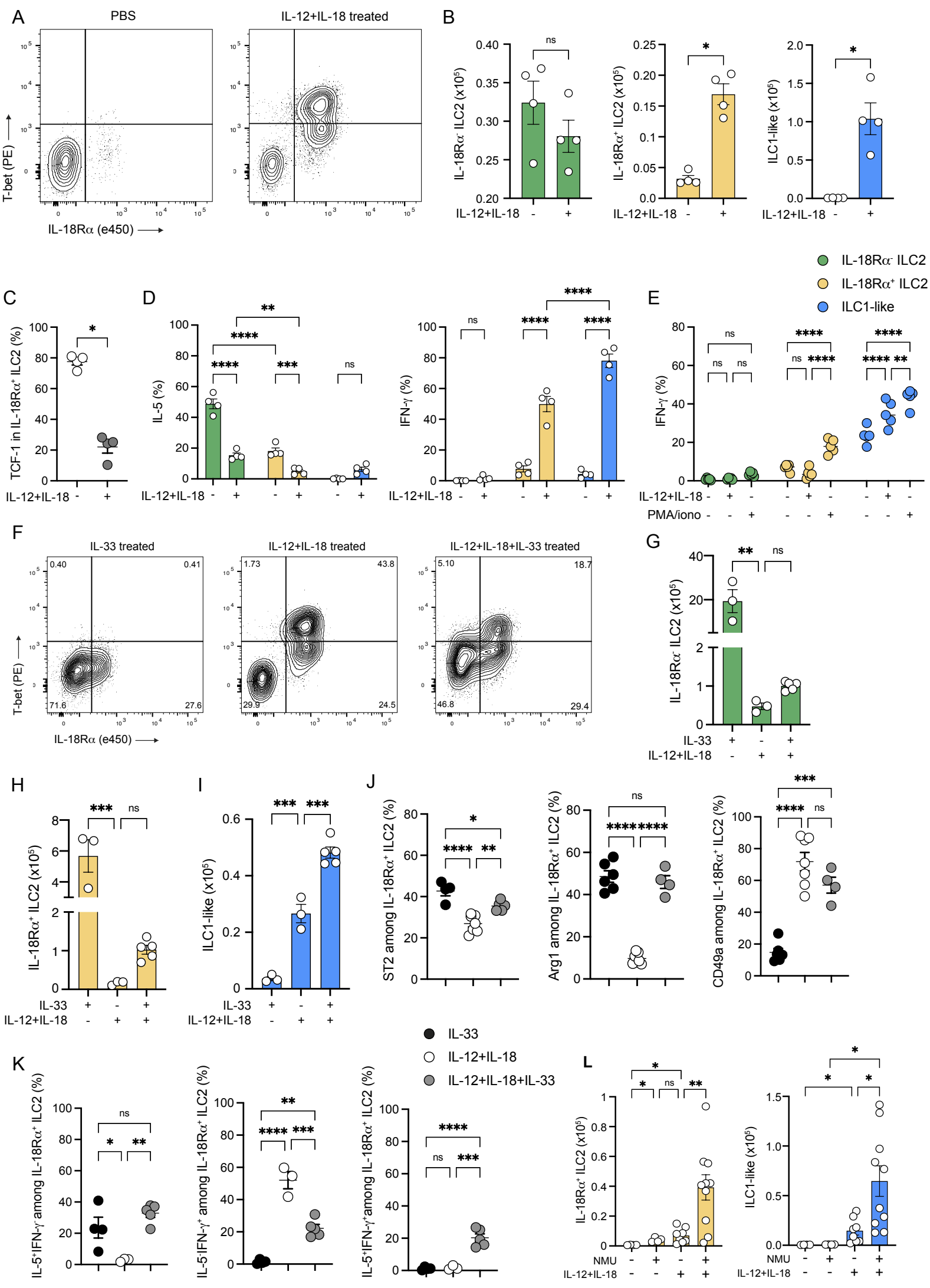
925 **Supplementary Figure 2. Combination of IL-12, IL-18 and IL-33 induces a mixed**  
926 **ILC1 and ILC2 phenotype on IL-18R $\alpha$ <sup>+</sup> ILC2. (A)** Representative dot-plot showing IL-  
927 5 and IL-18R $\alpha$  expression among IL-18R $\alpha$ <sup>-</sup> ILC2 (green), IL-18R $\alpha$ <sup>+</sup> ILC2 (red), and  
928 ILC1-like (blue) in PBS vs. IL-12+IL-18 treated IL-5<sup>Cre</sup>ROSA26<sup>YFP</sup> mic (left) and  
929 quantification (right). **(B)** Representative dot-plot showing YFP and IL-18R $\alpha$   
930 expression among IL-18R $\alpha$ <sup>-</sup> ILC2 (green), IL-18R $\alpha$ <sup>+</sup> ILC2 (red), and ILC1-like (blue) in  
931 PBS vs. IL-12+IL-18 treated IL-5<sup>Cre</sup>ROSA26<sup>YFP</sup> mic (left) and quantification (right). **(C)**  
932 Unsupervised t-SNE representation of the expression of different markers (GATA3,  
933 Arg1, T-bet, IL-18R $\alpha$ , CD49a, CD226 and Ki67) on Lin<sup>-</sup>CD45.2<sup>+</sup>CD90.2<sup>+</sup>NK1.1<sup>-</sup>ROR $\gamma$ t<sup>+</sup>  
934 in non-infected vs. *Mtb*-infected (28 dpi) vs. IL-12+IL-18 treated Rag2<sup>-/-</sup> mice. **(D)** As in  
935 A) except that the analysis was performed on Lin<sup>-</sup>CD45.2<sup>+</sup>CD90.2<sup>+</sup>NK1.1<sup>-</sup>ROR $\gamma$ t<sup>+</sup> in IL-  
936 12+IL-18 vs. IL-33 vs. IL-12+IL-18 treated Rag2<sup>-/-</sup> mice. Statistical analysis was  
937 performed two-way ANOVA test **(A-B)** (\*, p<0.05; \*\*, P<0.01; \*\*\*, p<0.001; \*\*\*\*,  
938 p<0.0001). Graphs depict data as mean ( $\pm$  s.e.m). Data are representative of two **(A-**  
939 **B)** independent experiments.

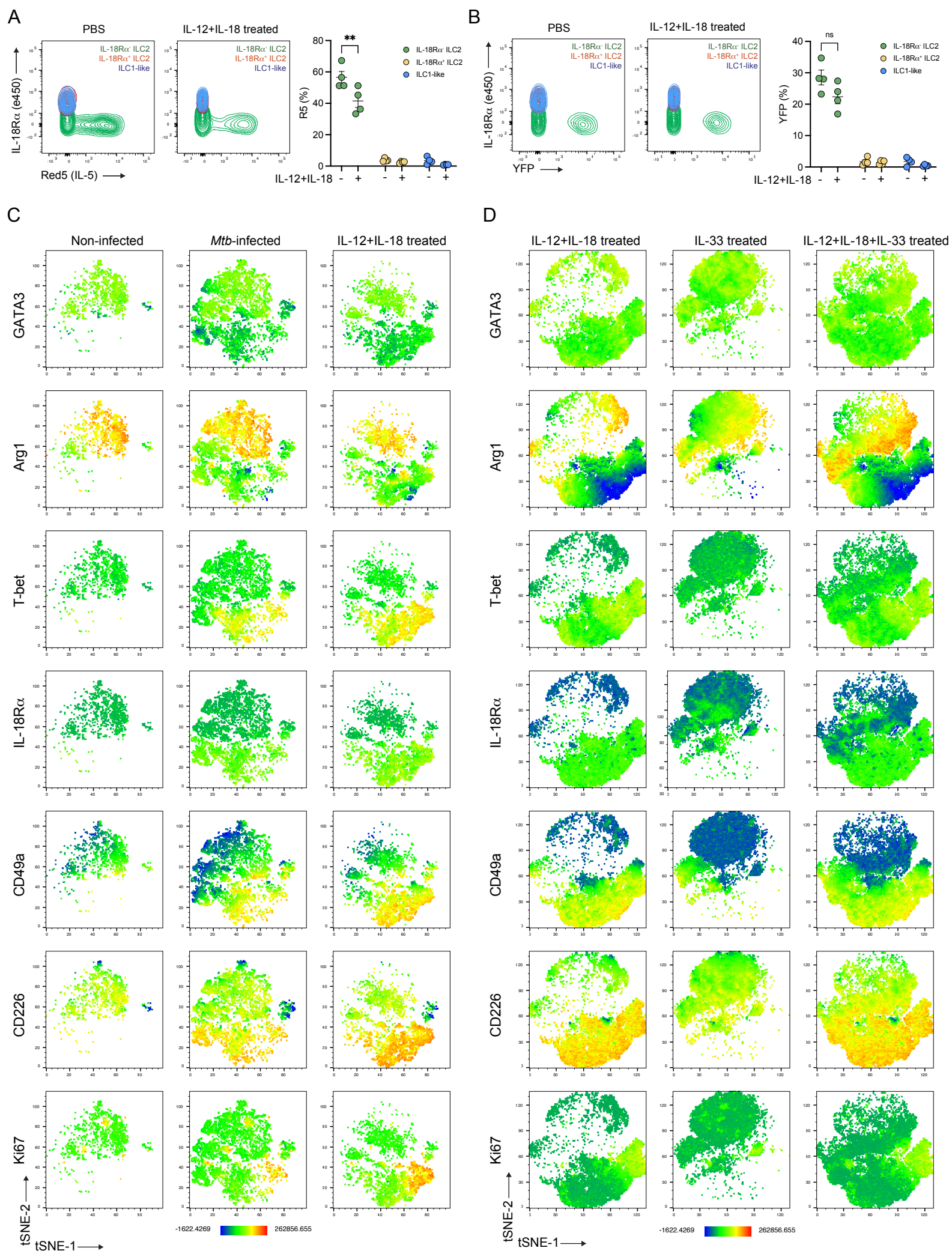
940 **Supplementary Figure 3. Glycolysis regulates ILC1-like cell differentiation**  
941 **during *Mtb* infection. (A)** Percentage of puromycin positive cells in ILC1 (dark blue),  
942 ILC3 (red), IL-18R $\alpha$ <sup>-</sup> ILC2 (green), IL-18R $\alpha$ <sup>+</sup> ILC2 (yellow) and ILC1-like cells (blue) in  
943 non-infected vs. *Mtb*-infected Rag2<sup>-/-</sup> mice. **(B)** HIF1 $\alpha$  expression in the indicated ILC  
944 subsets at day 28 post-infection **(C)** Expression of IFN- $\gamma$  in total ILCs after *ex vivo*  
945 stimulation with IL-12+IL-18 in the presence or absence of 2-DG. **(D)** Absolute  
946 numbers of ILC1-like cells in Rag2<sup>-/-</sup> mice treated or not with 2-DG during *Mtb* infection  
947 at day 28 post-infection. **(E)** Percentages of IFN $\gamma$ -producing cells among ILC1-like cells  
948 after *ex vivo* stimulation with PMA/ionomycin in the presence of brefeldin A for 4h from  
949 PBS vs. 2-DG treated mice. **(F)** As in **(D)** except that mice treated with 30% glucose in  
950 their drinking water. **(G)** As in **(E)** except that mice were treated or not with 30% glucose  
951 in their drinking water. Each symbol represents an individual mouse and statistical  
952 analysis was performed using two-way ANOVA **(A)**, one-way ANOVA **(B)**, Wilcoxon  
953 **(C)** and Mann-Whitney **(D-G)** tests (\*, p<0.05; \*\*, P<0.01; \*\*\*, p<0.001; \*\*\*\*, p<0.0001).  
954 Graphs depict data as mean ( $\pm$  s.e.m) from three **(D-E)** or two **(A-C, F-G)** independent  
955 experiments.

956 **Supplementary Figure 4. Metabolic regulation of IL-18R $\alpha$ <sup>+</sup> ILC2 differentiation**  
957 **into ILC1-like cells during *Mycobacterium tuberculosis* infection.** *Mtb* infection  
958 results in the establishment of a type 1 inflammation. Type 1 cytokines, IL-12, IL-18  
959 and IFN- $\gamma$  (upper part) act on a rare, lung immature IL-18R $\alpha$ -expressing ILC2 subset  
960 and triggers a glycolysis-involving metabolic reprogramming leading to its  
961 differentiation into ILC1-like cells IL18R $\alpha$ <sup>+</sup>, CD49a<sup>+</sup>CD226<sup>+</sup>HIF-1 $\alpha$ <sup>+</sup>, T-bet<sup>+</sup>, IFN- $\gamma$ -  
962 producing) endowed with a protective potential against *Mtb*. In contrast, type 2  
963 cytokines such as IL-33 (lower part) acts on this immature IL-18R $\alpha$ -expressing ILC2  
964 subset to drive its maturation toward mature IL-5 producing ILC2.

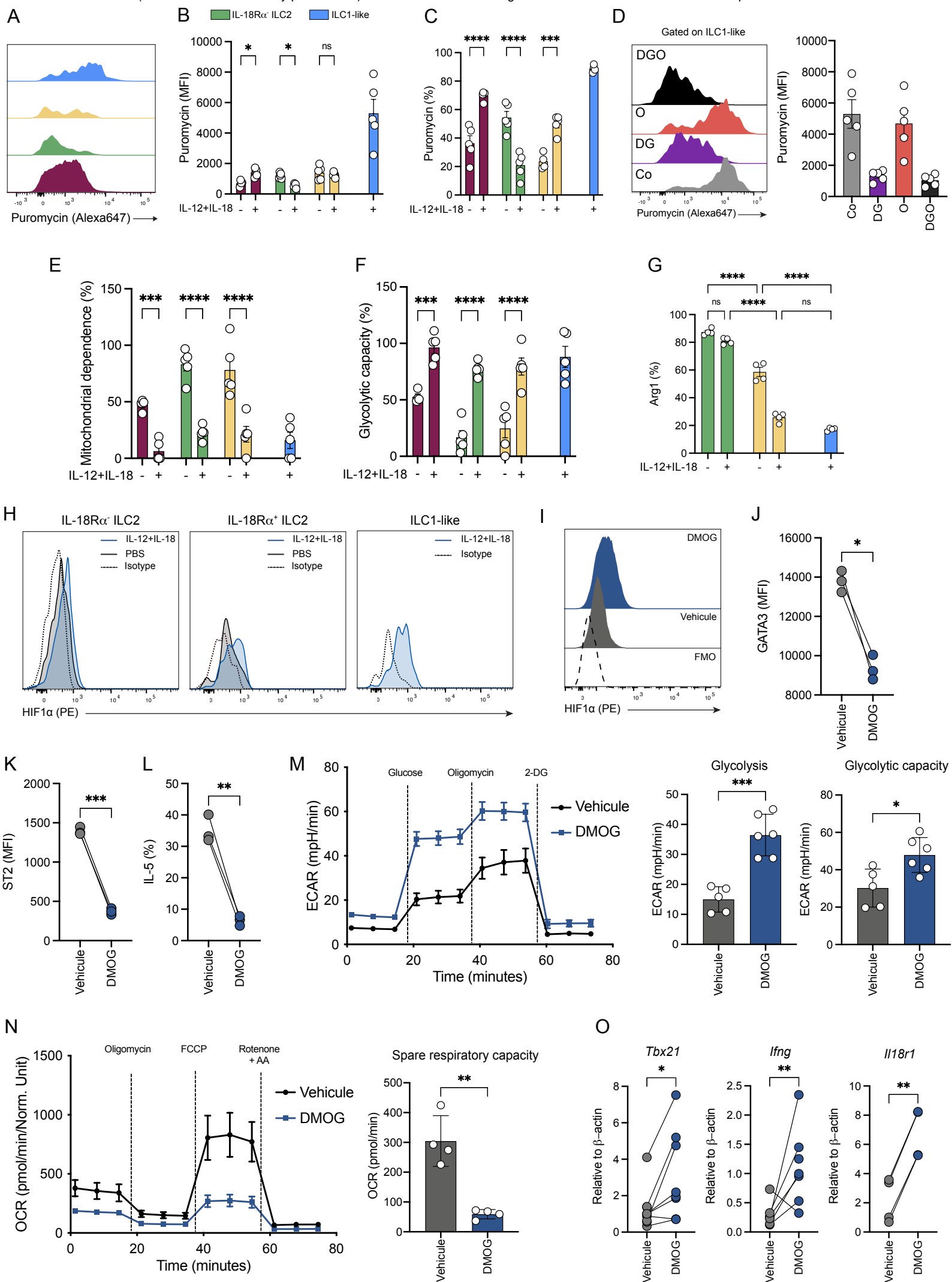


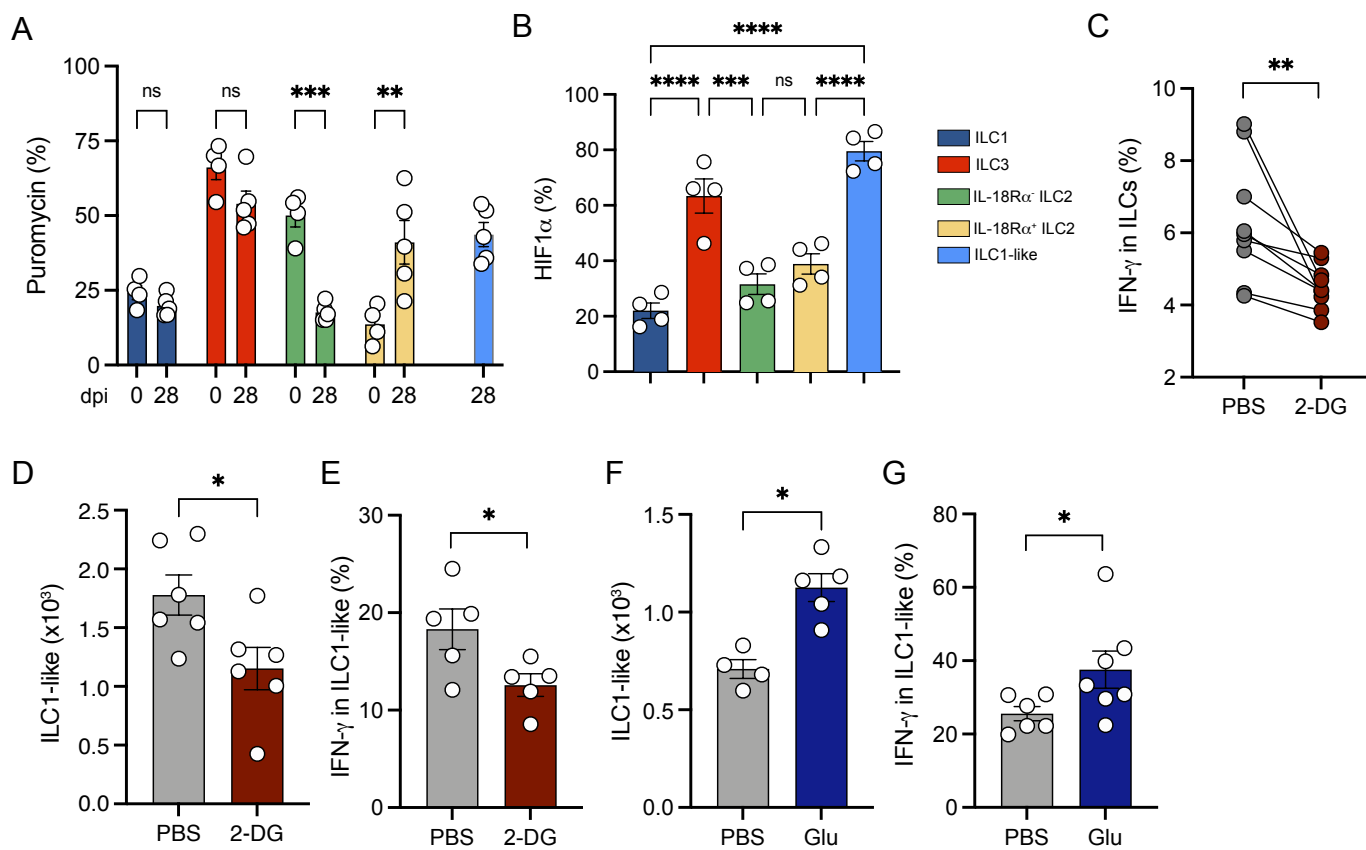


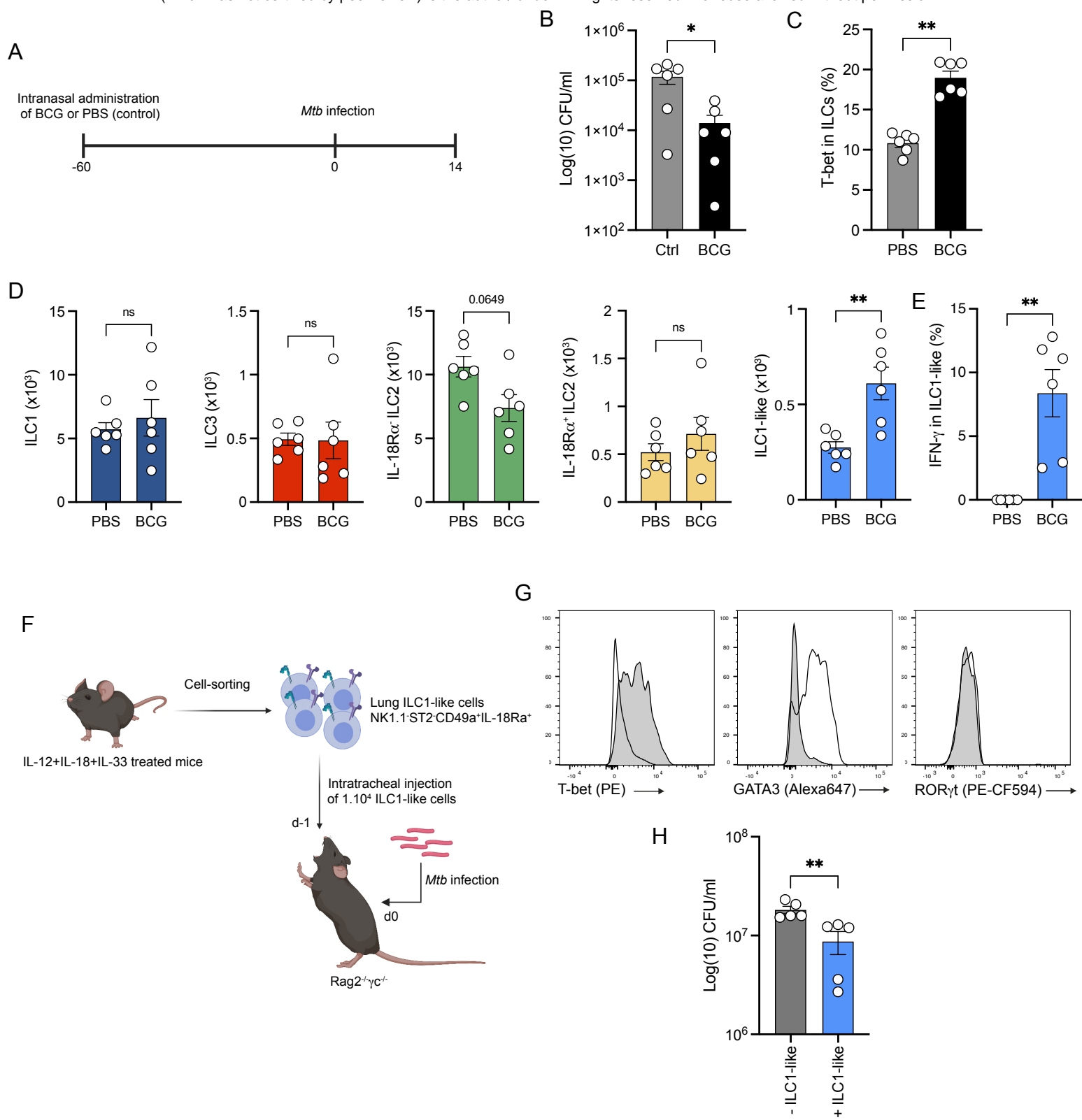












*Mycobacterium tuberculosis*

